NATÁLIA LEITE OLIVEIRA

INFRARED-ASSISTED FREEZE-DRYING (IRFD): EFFECT OF THE INFRARED RADIATION WAVELENGTH SECTION ON ENERGY CONSUMPTION AND QUALITY OF FREEZE-DRIED FRUITS

LAVRAS – MG
2023

NATÁLIA LEITE OLIVEIRA

INFRARED-ASSISTED FREEZE-DRYING (IRFD): EFFECT OF THE INFRARED RADIATION WAVELENGTH SECTION ON ENERGY CONSUMPTION AND QUALITY OF FREEZE-DRIED FRUITS

Tese apresentada à Universidade Federal de Lavras, como parte das exigências do Programa de Pós-Graduação em Ciência dos Alimentos para a obtenção do título de Doutor.

Prof. Dr. Jaime Vilela de Resende
Orientador

LAVRAS – MG
2023

Ficha catalográfica elaborada pelo Sistema de Geração de Ficha Catalográfica da Biblioteca Universitária da UFLA, com dados informados pelo(a) próprio(a) autor(a).

Oliveira, Natália Leite.
Infrared-assisted freeze-drying (IRFD): Effect of the infrared radiation wavelength section on energy consumption and quality of freeze-dried fruits / Natália Leite Oliveira. - 2022.
92 p.: il.

Orientador(a): Jaime Vilela de Resende.

Tese (doutorado) - Universidade Federal de Lavras, 2022.
Bibliografia.

1. Colapso. 2. Cinética de secagem. 3. Antocianinas. I. Resende, Jaime Vilela de. II. Título.

NATÁLIA LEITE OLIVEIRA

INFRARED-ASSISTED FREEZE-DRYING (IRFD): EFFECT OF THE INFRARED RADIATION WAVELENGTH SECTION ON ENERGY CONSUMPTION AND QUALITY OF FREEZE-DRIED FRUITS

SECAGEM POR LIOFILIZAÇÃO ASSISTIDA POR RADIAÇÃO INFRAVERMELHO (IR): EFEITOS DA IR SOBRE O CONSUMO DE ENERGIA E NA QUALIDADE DE FRUTAS LIOFILIZADAS

Tese apresentada à Universidade Federal de Lavras, como parte das exigências do Programa de Pós-Graduação em Ciência dos Alimentos para a obtenção do título de Doutor.

APROVADA em 24 de outubro de 2022.

Dr. Jaime Vilela de Resende	UFLA
Dr. Diego Alvarenga Botrel	UFLA
Drª. Ísis Celena Amaral	IFNMG
Drª. Lanamar de Almeida Carlos	UFSJ
Dr. Vivaldo Silveira Júnior	UNICAMP

_____

Prof. Dr. Jaime Vilela de Resende
Orientador

LAVRAS-MG
2023

À Deus por me confiar neste trabalho, aos meus pais Mileidy e Marco Aurélio e à minha irmã Renata por serem minha base e minha inspiração de vida.

Dedico

AGRADECIMENTOS

A escolha de realizar o mestrado e o doutorado foi algo do qual eu nunca havia imaginado quando comecei a graduação em Engenharia de Alimentos em 2011, mas ser professora sempre foi um sonho de criança. Em 2013, incentivada por uma grande amiga, Beatriz, passei no processo seletivo para começar a iniciação científica no Laboratório de Refrigeração de Alimentos sob orientação do professor Jaime Vilela de Resende - que durou dois anos. Neste tempo conheci pessoas maravilhosas que me mostraram o caminho da pesquisa e do ensino. Então resolvi ingressar no mestrado, também sob supervisão do professor Jaime e em seguida o doutorado. Toda essa trajetória só foi possível primeiramente à grandiosidade de Deus, por iluminar e guiar todos os meus caminhos. E aos meus pais e irmã, Mileidy, Marco Aurélio e Renata, por toda a confiança, incentivo, consolo e amor imensuráveis. Neste espaço também agradeço à toda família Oliveira e à família Leite, em especial aos meus avós, pelo exemplo de dedicação, honra e força. Agradeço também ao meu companheiro, Alexandre, por sempre abraçar meus sonhos e me ajudar em simplesmente tudo. Agradeço aos meus amigos de graduação, Ana Clara, Deza, Camila, Gabi, Beth, Bia, William e à minha eterna república Mina Mora por fazerem destes os melhores anos da minha vida. Agradeço aos meus companheiros de laboratório e grandes amigos, Adrise, Isabelle, Sérgio, Amanda, Ana Cristina, Iasmim, Ana Cláudia e Larissa, por todo o conhecimento, risadas, conversas e pesquisas realizadas. Também agradeço aos amigos, técnicos e professores do Departamento de Ciência dos Alimentos. Em especial, agraço ao meu orientador, professor Jaime, por toda a confiança, paciência e ensinamentos em todos estes anos. Agradeço ao apoio do programa de pós-graduação em Ciência dos Alimentos, à Universidade Federal de Lavras (UFLA), ao Conselho Nacional de Desenvolvimento Científico e Tecnológico (CNPq) e à Coordenação de Aperfeiçoamento de Pessoal de Nível Superior – Brasil (CAPES) pela estrutura, incentivo financeiro e por permitirem o doutorado sanduíche na *University of Guelph*. Agradeço ao meu orientador estrangeiro, Michael Rogers, pela confiança, recepção e ensinamentos. Agradeço também aos professores Diego, Ísis, Lanamar e Vivaldo pela disponibilização em participar da banca e pela contribuição ao trabalho. Agradeço a todos que fizeram com que estes mais de 10 anos na Universidade Federal de Lavras fossem mais do que especiais – a escrita desta tese não seria a mesma sem todos os que passaram por mim e deixaram um pouquinho do conhecimento, da alegria e amor comigo.

RESUMO

A liofilização assistida por radiação infravermelha (IRFD) é um método promissor para otimização do tempo de secagem. A presente tese objetivou determinar qual a seção do comprimento de onda da radiação infravermelha (IR) é ideal para secagem de frutas. Para isto, acoplou-se ao topo da cuba de secagem um bocal para inserção da lâmpada IR e inseriu-se um sistema de aquisição de dados para acompanhar a temperatura e a massa dos produtos ao longo do tempo. A pesquisa foi dividida em dois artigos, no artigo 1 avaliou-se a secagem e qualidade final da polpa de açaí em pó. Neste, os tratamentos para secagem da polpa foram: liofilização tradicional (FD); IRFD no comprimento de onda próximo (NIRFD); IRFD no comprimento de onda distante (FARFD); e aquecimento infravermelho após redução de peso de 20%, $NIRFD_{20\%WR,}$ e $FARFD_{20\%WR}$. A secagem por IRFD reduziu significativamente o tempo total de processo, com NIRFD e FARFD reduzindo em 49,42% e 33,40%, respectivamente, o tempo de secagem comparado ao FD. A estrutura do pó utilizando IR mostrou-se mais aberta e com poros maiores. $FARFD_{20\%WR}$ apresentou células colapsadas que comprometeram as propriedades tecnológicas do pó (molhabilidade, dispersibilidade). Para compostos bioativos, o conteúdo fenólico total (TPC) não foi afetado pela IR, $p>0,05$, variando de 963,44 a 1025,60 mg/100 g. A capacidade antioxidante aumentou (59,91 para 88,06%) quando o infravermelho distante foi utilizado devido a reação de Maillard que gerou compostos antioxidantes e produto mais escuro. O teor de antocianinas reduziu em amostras secas com a lâmpada FAR. Já no artigo 2, o experimento consistiu na secagem de amora-preta inteira (*Rubus* spp.) utilizando os tratamentos FD; NIRFD; FARFD, e incorporação da IRFD após 40% de redução na massa: $NIRFD_{40\% WR}$ e $FARFD_{40\% WR}$. O tratamento NIRFD foi o mais rápido devido à capacidade de penetração desta seção de comprimento de onda ser maior, com redução de 42.51% do tempo de secagem (17,2 h), seguido pelo FARFD com 36,5% (18,9 h) comparado com o FD (29,9 h). As amoras apresentaram coloração característica, $p>0.05$, L* 17,5, a* 17,6, b* 11,3 e h^o 32,9, indicando a cor vermelha. Amoras-pretas secas obtidas por FARFD e $FARFD_{40\%WR}$ apresentaram maior dureza, 10,13 N, em comparação com FD, 6,98 N. Este resultado influenciou na reidratação, onde FARFD obteve as menores razões de reidratação (RR) devido às partes mais densas na camada externa dessas frutas. Já o NIRFD mostrou os maiores valores para RR em todo o tempo analisado. Maiores capacidades antioxidantes foram obtidas nos tratamentos onde a secagem foi mais rápida em NIRFD e FARFD com 77,91 e 77,37%, respectivamente. Por fim, os resultados de ambos os estudos mostraram que a secagem por IRFD exibiu bom potencial para a produção de frutas secas em pó ou inteiras quando utilizado o comprimento de onda próximo, NIRFD, apresentando produtos com boa aparência, alto conteúdo nutricional e manutenção das propriedades tecnológicas.

Palavras-chave: Antocianinas. Cinética de secagem. Colapso.

ABSTRACT

Infrared radiation-assisted freeze-drying (IRFD) is a promising method for time optimizing. The present thesis aimed to determine which section of the infrared radiation (IR) wavelength is ideal for drying fruits. For this, infrared lamp was attached to the top of the drying chamber. The temperature and weight reduction were monitoring during the time using thermocouples and a scale, respectively, both coupled to the data acquisition system. The research was divided into two papers, in article 1 the drying and final quality of the açaí pulp powder were evaluated. In this article, the treatments for pulp drying were freeze-drying control treatment, FD; freeze-drying and continuous near infrared radiation heating, NIRFD; freeze-drying and near infrared radiation heating after 20% weight reduction, $NIRFD_{20\%WR}$; freeze-drying and continuous far infrared radiation heating, FARFD; freeze-drying and far infrared radiation heating after 20% weight reduction, $FARFD_{20\%WR}$. IRFD significantly reduced the total drying time, with NIRFD and FARFD taking 49.42% and 33.40% less time than FD, respectively. The structure of powdered using IRFD was more open and with larger pores. $FARFD_{20\%WR}$ had collapsed cells that compromised the functional properties of the powder (wettability, dispersibility). As for bioactive compounds, phenolic content was not affected by IRFD, ranging from 963.44 to 1025.60 mg/100 g. Antioxidant capacity increased (59.91 to 88.06%) when far infrared was used due to a Maillard reaction that generated antioxidant compounds and darker product. Content of anthocyanins reduced in samples dried by far infrared. In article 2, the experiment consisted of drying whole blackberry (Rubus spp.) using FD treatments; NIRFD; FARFD, and incorporation of IRFD after 40% in weight reduction: $NIRFD_{40\% WR}$ and $FARFD_{40\% WR}$. The NIRFD treatment was also the fastest due to the penetration capacity of this wavelength section being higher, with a 42.51% reduction in drying time (17.2 h), followed by FARFD with 36.5% (18.9 h) compared to FD (29.9h). Blackberries had good final appearance and characteristic red color, $p>0.05$, L* 17.5, a* 17.6, b* 11.3 and h^o 32.9. Samples obtained using long-wave had higher hardness (10.13 N) compared to FD (6.98 N). This result influenced negatively rehydration ratio. Also, these treatments reduced the anthocyanins content. On the other hand, NIRFD samples had the highest values for RR throughout the entire time evaluated. Higher antioxidant capacities (AC) were obtained in treatments with shorter drying times, with NIRFD and FARFD having AC values of 77.91 and 77.37%, respectively. Finally, both articles showed that IRFD drying exhibited good potential for the production of powdered or whole dried fruits when using the short wavelength, NIRFD, presenting products with good appearance, high nutritional content and maintenance of technological properties.

Keywords: Anthocyanins. Drying kinetics. Collapse.

LISTA DE FIGURAS

PRIMEIRA PARTE

SEGUNDA PARTE

Artigo 1

Artigo 2

LISTA DE TABELAS

Artigo 1

Artigo 2

SUMÁRIO

PRIMEIRA PARTE

1 INTRODUÇÃO

Alimentos liofilizados apresentam alta qualidade quando comparados aos produtos secos por outros métodos de secagem. Isto se deve à manutenção da estabilidade e das propriedades sensoriais e nutricionais. Ademais, devido à baixa atividade de água, possuem longa vida útil à temperatura ambiente (~1 ano) e se destacam pelo fácil preparo e reconstituição (quando necessário). De acordo com as características mencionadas e com o crescimento da procura do consumidor por produtos seguros, práticos e ricos nutricionalmente, o mercado de produtos liofilizados na indústria de alimentos deve aumentar em US$ 31,26 bilhões de 2020 a 2025, com uma taxa de crescimento anual de 9% (TECHNAVIO, 2021).

Por outro lado, este processo possui como desvantagem o elevado custo operacional (congelamento, vácuo, aquecimento das prateleiras) que faz com que os produtos liofilizados sejam caros e se justifiquem apenas quando há um alto valor agregado. Com isso, pesquisas vêm sendo realizadas para reduzir os gastos operacionais sem afetar a qualidade do produto final. Dentre estas, tem-se a introdução da radiação infravermelha (IR), em substituição ao aquecimento elétrico, com objetivo de acelerar a sublimação. Este método é chamado de liofilização assistida por radiação infravermelha (IRFD).

Na secagem por IRFD, a IR fornece energia diretamente para a superfície do material e, portanto, causa seu rápido aquecimento gerando maior eficiência térmica e taxa de aquecimento mais rápida em comparação com o aquecimento convencional. A IR é propagada como ondas eletromagnéticas abrangendo os comprimentos de onda de 0,75 a 1.000 μm. Este espectro é dividido em três seções, a saber: IR próximo (NIR) (0,78–1,4 μm), IR médio (MIR) (1,4–3,0 μm) e IR distante (FAR) (3,0– 1000 μm).

Estudos utilizando aquecedores com comprimentos de onda próximo, médio e distante mostraram que a IRFD é capaz de encurtar o período de secagem. Autores relataram que utilizando a IR no comprimento de onda próximo, esta é transmitida através da água, enquanto utilizando o comprimento de onda distante, a radiação é absorvida na superfície. Entretanto, não há na literatura estudos comparando às seções do infravermelho na IRFD. Diante disso, o presente estudo teve como objetivos construir uma câmara de secagem com a adição de lâmpada infravermelho na seção do comprimento de onda distante (FAR) ou próximo (NIR) para avaliar qual é ideal para a secagem de frutas em polpa (açaí), artigo 1, e fruta inteira (amora-preta), artigo 2, analisando questões econômicas, nutricionais e tecnológicas.

2 REFERENCIAL TEÓRICO

2.1 Secagem de frutas

As frutas são importantes constituintes da nutrição humana, apresentando benefícios potenciais para a saúde, sendo fontes preciosas de nutrientes, como fibras, vitaminas, minerais e inúmeros compostos bioativos (XU et al., 2022). Entretanto, frutas frescas possuem elevado teor de água e carboidratos de baixo peso molecular, especialmente a frutose, glicose e sacarose, que são facilmente fermentáveis levando à deterioração (SVIECH; UBBINK; PRATA, 2022).

A deterioração desses frutos é muitas vezes iniciada por injúrias, visto que são frutos altamente sensíveis por apresentarem peles muitas vezes finas e de textura macia (SVIECH; UBBINK; PRATA, 2022). Dessa forma, a distribuição de frutas frescas para locais longes do centro de produção pode ser um desafio. Especialistas da *Food and Agriculture Organization* sugerem que o aprimoramento e o uso de técnicas de preservação pode trazer vantagens ambientais, econômicas e sociais (FAO, 2019).

Dentre os métodos de preservação, a secagem é usada para reduzir a atividade de água dos alimentos aumentando a estabilidade de armazenamento. Este método minimiza a necessidade de embalagem e reduz o peso do transporte. Além disso, a secagem faz com que novos produtos alimentícios sejam gerados como, por exemplo, frutas e vegetais secos ou na versão em pó (SALEHI; AGHAJANZADEH, 2020).

As frutas secas são popularmente consumidas como *snacks* devido ao sabor mais adocicado, à praticidade e também pelas muitas propriedades nutricionais e funcionais que oferecem. Já frutas e vegetais em pó vem sendo utilizados como ingredientes em produtos para panificação, uma vez que auxiliam na melhora dos valores nutricionais, aspectos físicos, sensoriais e atributos microbiológicos dos produtos (JESZKA-SKOWRON; CZARCZYŃSKA-GOŚLIŃSKA, 2020; SALEHI; AGHAJANZADEH, 2020).

Na indústria alimentícia, existem diferentes tecnologias para secar frutas e hortaliças, como secador solar, aquecimento por microondas, irradiação infravermelha, secagem a vapor superaquecido, secagem fluidizada, secagem instantânea, liofilização e secagem a vácuo (SAGAR; SURESH KUMAR, 2010). O sistema de secagem aplicado tem papel fundamental no teor de umidade final, na qualidade e vida útil do pó obtido (SALEHI; AGHAJANZADEH, 2020; SALEHI; KASHANINEJAD, 2018). Portanto, os parâmetros de secagem como o capital a ser investido, consumo de energia, qualidade dos produtos secos e mercado são importantes para seleção do processo.

2.2 Liofilização

Processo

A liofilização é um processo de desidratação que se fundamenta na remoção do solvente por sublimação (transição direta do estado sólido para o estado gasoso). Este processo data dos tempos pré-históricos, quando os esquimós preservavam peixes por desidratação nos ventos frios do Ártico. Entretanto, devido à complexidade dos processos de secagem por congelamento, a industrialização da liofilização começou de fato na década de 1930, quando surgiu a necessidade de preservar grandes volumes de hemoderivados sensíveis ao calor e antibióticos recém-descobertos (ASSEGEHEGN et al., 2020).

A secagem por liofilização pode ser compreendida através do diagrama de fases da água, Figura 1, onde a linha de sublimação é colocada a temperaturas inferiores ao ponto triplo da água (Temperatura = 0.01 °C, Pressão< 4580 mTorr ou 612 Pa). Dessa forma, para atravessar a linha de sublimação, conforme necessário para a liofilização, o produto, inicialmente nas condições ambientais, ponto A na Figura 1, deve ser congelado. Ou seja, a temperatura deve reduzir, passando para os pontos B e C na Figura 1. A pressão de vapor de água deve descer abaixo da pressão correspondente ao ponto triplo e, por fim, algum calor deve ser fornecido para converter o gelo em vapor por sublimação, ponto D na Figura 1 (BERK, 2018; FELLOWS, 2017; RATTI, 2013).

Figura 1 – Diagrama de fases da água.

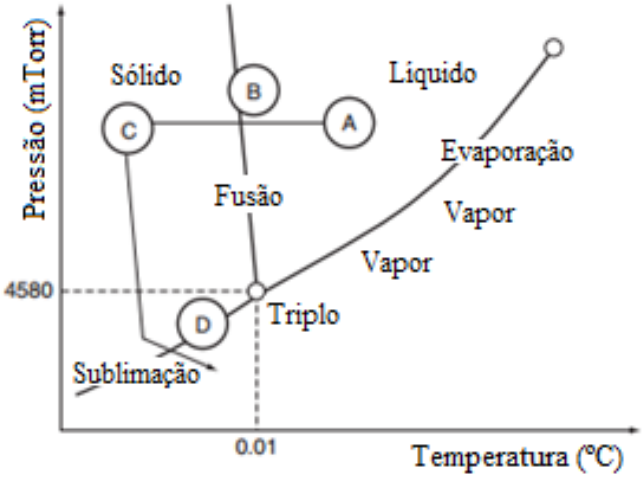

Fonte: Ratti (2013).

Assim, pode-se dizer que a liofilização é a combinação de dois processos igualmente importantes: o congelamento, durante o qual a maior parte do solvente, até 95% (TANG; PIKAL, 2004), é convertido em um sólido congelado, e a secagem, durante a qual quase todo o solvente (congelado e descongelado) é removido da formulação.

No congelamento a maior parte da água converte-se em gelo. O produto congelado é formado por duas fases: o gelo e o concentrado residual. À medida que a temperatura é reduzida mais cristais de gelo são formados e o soluto fica cada vez mais concentrado, até um máximo acima do qual um aumento adicional na concentração não é possível (BANSAL; LALE; GOYAL, 2012). No ponto de formação máximo de gelo, o concentrado residual solidifica entre os cristais de gelo que compõem a matriz (BANSAL; LALE; GOYAL, 2012). Neste estado, o soluto é denominado como um "soluto com concentração máxima de congelamento", que é a fase vítrea e/ou cristalina do produto congelado (RAMBHATLA et al., 2004). A morfologia da matriz congelada depende da taxa de resfriamento, da concentração inicial, da temperatura final de resfriamento e do tempo a esta temperatura. O congelamento pode ocorrer usando um congelador externo ou diretamente na câmara do liofilizador, quando este permite.

Após o congelamento inicia-se o processo de secagem que é dividido em duas etapas, a saber, sublimação (secagem primária) e dessorção (secagem secundária) (ASSEGEHEGN et al., 2020). A secagem primária consiste no aquecimento da amostra sob condições de vácuo parcial, sempre abaixo do ponto triplo, para forçar a sublimação do gelo. Nesta etapa ocorre a sublimação dos cristais de gelo, proporcionando um produto com estrutura porosa que, pode ser, posteriormente, reidratado, preservando as características sensoriais e propriedades nutricionais do produto original (BERK, 2009; RATTI, 2013). A secagem primária é a mais longa do ciclo e condiciona na maioria das propriedades relacionadas à qualidade do produto.

Durante a secagem primária, a sublimação do gelo libera quantidades significativas de vapor d'água, o que leva ao aumento instantâneo da pressão da câmara. Se este vapor não for removido, o sistema atinge o equilíbrio dinâmico e a sublimação do gelo cessa, pois o solvente requer que a pressão no liofilizador seja menor, ou próxima, à pressão de vapor de equilíbrio do solvente congelado (PITTIA; ANTONELLO, 2015). Dessa forma, a remoção contínua do vapor d'água é vital para a continuidade da sublimação de gelo, a qual ocorre por meio do condensador de gelo disposto no liofilizador. Qualquer vapor d’água disponível é imediatamente convertido em gelo nas bobinas do condensador por meio de um processo conhecido como sublimação inversa ou deposição. Portanto, além da remoção contínua de

vapor d'água durante a secagem primária, a taxa e a capacidade de deposição de gelo são igualmente importantes (ASSEGEHEGN et al., 2020).

Para formulações amorfas, após a conclusão da secagem primária, a quantidade de água residual é significativamente alta e pode afetar a estabilidade de armazenamento. Esta água restante é atribuída à água não congelada que permanece adsorvida dentro da matriz de soluto e pode estar presente em quantidades de 5–20% do teor de água inicial, dependendo do teor de sólidos da formulação (ASSEGEHEGN et al., 2020; TANG; PIKAL, 2004).

Quando a maior parte do gelo (água livre) sublimou, a água ligada deixará o produto por dessorção, sendo esta etapa denominada secagem secundária. A secagem secundária começa enquanto a sublimação ainda está a ocorrer, porém é predominante apenas no final da liofilização quando cessa a sublimação (DUROUDIER, 2017; FERESHTEH, 2018). Sendo estes, os seguintes processos que ocorrem durante um processo de dessorção completo: (1) difusão da água adsorvida da matriz interna de um sólido amorfo para a superfície do sólido, (2) evaporação da água do sólido superfície e (3) transporte de vapor do interior do produto seco para o condensador de gelo (FELLOWS, 2017; PIKAL et al., 1990).

A secagem secundária (dessorção/evaporação) ocorre com velocidade menor que a sublimação, já que a umidade do produto é menor e a água não está livre (5% a 20% do total de água do material) (FELLOWS, 2009, 2017). A finalização desta etapa somente deve ocorrer quando a umidade residual for tão pequena quanto a que o material necessite para manter sua estabilidade e qualidade por longo tempo, garantindo um processo de secagem por liofilização eficiente (ASSEGEHEGN et al., 2020; MUJUMDAR; LAW; WOO, 2015; PAWAR; PRATAPE, 2017).

O processo de liofilização ocorre em liofilizadores que constam de câmara de vácuo ou cuba de liofilização, fonte de calor, condensador e bomba de vácuo (ORDONEZ, 2005). A câmara de vácuo é o local onde coloca-se o produto a ser seco. Neste espaço a pressão é reduzida para que não ocorra fusão do gelo. A fonte de calor tem como objetivo suprir o calor latente de sublimação. O condensador é constituído por serpentinas de refrigeração que transformam os vapores diretamente em gelo (executando a chamada sublimação inversa), sendo este adaptado com dispositivos automáticos de descongelamento a fim de manter área máxima de serpentina livre para que obtenha uma maior eficiência do processo. A bomba de vácuo tem a finalidade de remover os vapores não condensáveis (BERK, 2009; FELLOWS, 2009). E, o modo de operação pode ser em batelada ou contínuo.

2.3 Perfil de temperatura na liofilização

O perfil de temperatura do produto durante o congelamento e secagem (primária e secundária) no processo de liofilização está representado na Figura 2. Primeiro, o produto é congelado passando do ponto A para o B durante algum tempo, até ser completamente congelado. Em seguida, o vácuo e o aquecimento são aplicados, ponto C, para favorecer a secagem primária, parte D. Nesta etapa tem-se um processo endotérmico, a temperatura do produto permanece baixa, mesmo com a temperatura da prateleira acima de 0 °C (273.15 K) devido ao enorme calor de sublimação do gelo (50911 J/mol). Finalmente, quando o gelo é completamente sublimado, o produto aumenta acentuadamente a sua temperatura durante a secagem secundária, parte E, até atingir 2-3 ºC abaixo da temperatura da prateleira de aquecimento (RATTI, 2013).

Figura 2 – Processo de liofilização.

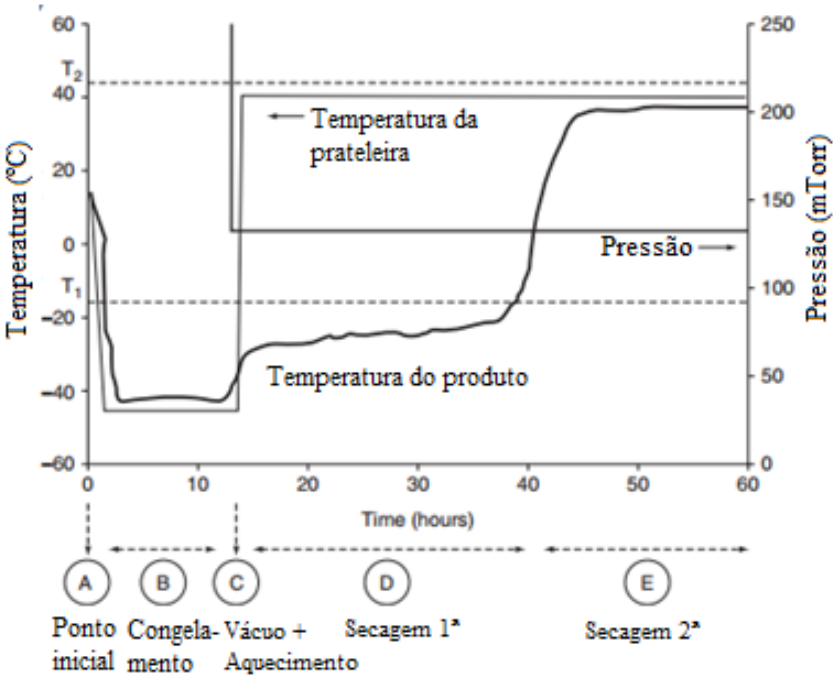

Fonte: Ratti (2013).

A temperatura máxima durante a secagem secundária é limitada por: (1) a sensibilidade à temperatura dos componentes da formulação, alguns dos quais podem perder suas propriedades terapêuticas ou outras funcionalidades em altas temperaturas de processamento, e (2) a temperatura de transição vítrea (T_g) da formulação, principalmente para formulações

amorfas. Devido à quantidade significativa de água restante após a finalização da secagem primária, a T_g do produto é muito baixa. Portanto, tanto a taxa de aquecimento quanto a temperatura final de secagem durante a secagem secundária devem ser escolhidas cuidadosamente para que a temperatura real do produto sempre fique abaixo da temperatura de transição vítrea momentânea (ASSEGEHEGN et al., 2020).

2.4 Transferência de calor e massa

A secagem por liofilização, assim como em outros processos de desidratação, envolve a transferência de calor e massa simultâneos. Como diferença, tem-se a distribuição do conteúdo de umidade no material, onde não é observada a presença de um perfil contínuo do conteúdo de água. Idealmente, observa-se duas zonas distintas: o núcleo congelado (com teor de água inicial) e uma camada seca (baixo teor de água, desprovida de cristais de gelo e apenas com a água adsorvida na matriz sólida), estes são divididos por uma interface chamada "frente de sublimação", Figura 3 (BERK, 2018; FELLOWS, 2017).

Figura 3 – Distribuição de umidade em um material submetido a liofilização.

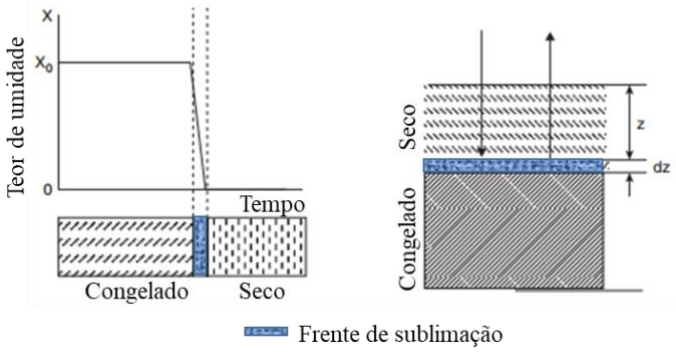

Fonte: Adaptado de Berk (2009).

Para que ocorra a remoção de água do produto, deve-se ter o fornecimento de calor ao material. O calor fornecido ao material congelado deve ser igual ao calor requerido pela sublimação para que a temperatura e a pressão da superfície de sublimação tornem-se estáveis e o processo de sublimação prossiga-se normalmente (HUA; LIU; ZHANG, 2010). O calor fornecido à frente de sublimação se dá por vários mecanismos, sendo a radiação e a condução os mais comumente aplicados (GARCIA-AMEZQUITA et al., 2015).

Na radiação, a transferência de calor é fornecida através de uma placa superior até a superfície exposta do material e, em seguida, este calor é conduzido através da zona seca para

a frente de sublimação, Figura 4. Com isso, a temperatura e a pressão de vapor do gelo aumentam e o vapor de água é liberado; este, então, se desloca através da zona seca, na direção oposta do fluxo de calor, da frente de sublimação para a superfície e desta para o condensador (BERK, 2018; FELLOWS, 2017; HUA; LIU; ZHANG, 2010).

Na condução, a transferência de calor ocorre por meio do contato das bandejas que contêm o material congelado com as prateleiras aquecidas do liofilizador. Dessa forma, o calor é transferido para a frente de sublimação por condução através da camada congelada. E, o vapor de água é transferido através da camada seca como descrito anteriormente (BERK, 2018; FELLOWS, 2017).

Figura 4 – Mecanismos de transferência de calor e massa na liofilização.

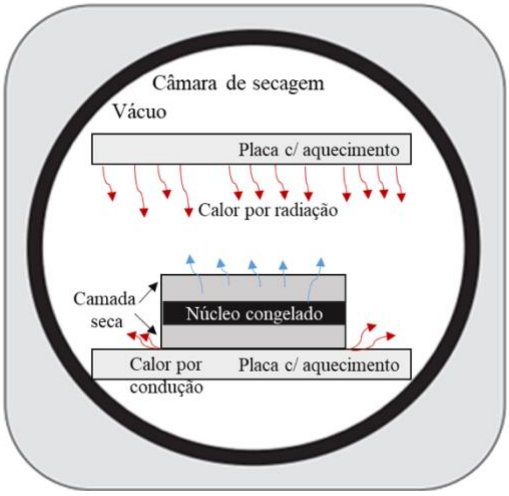

Fonte: Adaptado de Ratti (2013).

A transferência de calor no processo de liofilização pode ser analisada de forma unidimensional, uma vez que o diâmetro do material é maior que a altura deste (BERK, 2009, 2018). Dessa forma, a taxa de fornecimento de calor (q) é dada pela Equação 1:

$$q = A\rho_i(w_i - w_f)\lambda_s \frac{dz}{dt} \tag{1}$$

onde A é a área da superfície (m^2); ρ_i é a densidade do material congelado ($kg \cdot m^{-3}$); w_i, w_f são o conteúdo de água inicial e final respectivamente ($kg \cdot kg^{-1}$); λ_s ($J \cdot kg^{-1}$) é o calor latente de sublimação e $\frac{dz}{dt}$ é a relação entre a variação na espessura do material ao longo do tempo.

Para a análise da transferência de massa, durante a secagem primária, o gelo começa a sublimar da superfície do produto congelado em contato com as fontes de aquecimento,

formando uma camada seca com uma estrutura porosa. À medida que a liofilização prossegue, a frente de sublimação recua para o centro do produto, deixando a camada seca com uma espessura crescente contínua. Este aumento representa uma resistência à passagem de vapor de água, dessa forma, conforme ocorre a secagem, a taxa de transferência de massa diminui. Assim, um parâmetro importante para avaliar a dificuldade de transferência de massa durante a liofilização é a resistência da camada seca, conforme mostrado na Equação 2 (TANG; PIKAL, 2004):

$$\frac{dm}{dt} = \frac{P_{gelo} - P_{câmara}}{R_p} \quad (2)$$

em que $\frac{dm}{dt}$ é a taxa de sublimação, P_{gelo} e $P_{câmara}$ é a pressão do gelo na frente de sublimação e a pressão da câmara do liofilizador, respectivamente, e R_p é a resistência da camada seca.

A resistência do material seco depende da composição, concentração, porcentagem de sólidos, bem como as condições de congelamento. Uma alta resistência da camada seca, *Rp*, aumenta a temperatura do produto e retarda a secagem primária. Sendo que, a temperatura do produto deve permanecer abaixo de determinados limites, para evitar a deterioração da qualidade do produto, porém deve ser suficientemente elevada para ter uma taxa de sublimação/ dessorção considerável e evitar um processo lento e dispendioso (RATTI, 2013).

2.5 Vantagens e desvantagens da liofilização

Quando a secagem por liofilização é realizada de forma adequada, os produtos alimentares gerados possuem qualidade superior a outros métodos de secagem (PAN; ATUNGULU, 2010).

Dentre as razões para o sucesso da liofilização pode-se destacar que esta possui efeito benéfico na estabilidade de produtos ativos sensíveis ao calor e substâncias bioativas, reduz a desnaturação oxidativa e as reações degradativas, reduz o encolhimento dos alimentos, preserva as propriedades sensoriais, tais como, cor, aroma, sabor e aparência (GEORGE; DATTA, 2002). E, paralisa, em grande parte, as reações microbiológicas devido à redução na atividade de água (a_w) dos produtos, sendo que o ideal é $a_w < 0{,}4$ (RATTI, 2013). Ademais, os produtos

podem ser armazenados à temperatura ambiente e possuem reconstituição completa e rápida do produto seco no ponto de uso, pois a estrutura dos poros apresenta boa permeabilidade, proporcionando um alimento mais próximo ao alimento original (ASSEGEHEGN et al., 2020; KROKIDA; PHILIPPOPOULOS, 2006). Estas características são proeminentes das baixas temperaturas empregadas no processo que mantem a estrutura do produto durante a sublimação (PAN; ATUNGULU, 2010). Também, pode-se ressaltar o amplo reconhecimento e aceitação de produtos liofilizados no mercado (ASSEGEHEGN et al., 2020).

Para produtos alimentícios, a liofilização é utilizada principalmente no processamento do café instantâneo, em produtos alimentícios de alta qualidade, como especiarias e ervas, nos alimentos para esportes radicais, nas fórmulas instantâneas para bebês, nos compostos alimentares encapsulados e microrganismos. Recentemente, o mercado de produtos "naturais" e "orgânicos" tem aumentado, bem como as demandas dos consumidores por ingredientes e alimentos saudáveis com processamento mínimo e alta qualidade, o que justifica o uso da liofilização (FELLOWS, 2017; MUJUMDAR; LAW; WOO, 2015; WAGHMARE et al., 2021). Para a produção de microrganismos em pó na indústria, a liofilização é a técnica de secagem preferida, uma vez que causa menor perda de viabilidade celular quando comparada a outros métodos de secagem (MORGAN et al., 2006).

Como desvantagem, a liofilização é um processo demorado e caro tanto nos custos operacionais quanto de capital (ASSEGEHEGN et al., 2020). Em escala industrial, o custo operacional do processo de liofilização é da ordem de quatro a cinco vezes maior do que o custo operacional da técnica de secagem por pulverização e oito a dez vezes maior que do evaporador de estágio único (BERK, 2018; FELLOWS, 2017; KHALLOUFI; RATTI, 2003; PAN; ATUNGULU, 2010; WAGHMARE et al., 2021). Portanto, o processo de liofilização é normalmente usado para produtos de alto valor agregado que justifiquem os altos custos de fabricação.

2.6 Liofilização assistida por radiação infravermelha

A liofilização é um método de secagem bem aceito devido às excelentes características do produto gerado, entretanto ainda é caro devido à todas as etapas do processo (congelamento, aquecimento e vácuo), o que limita suas aplicações. Para contornar este problema, técnicas estão sendo desenvolvidas combinando ou modificando o processo de liofilização, dentre estas pode-se citar a liofilização assistida por radiação infravermelha (IRFD), com objetivo de torná-

la mais econômica em termos de tempo e, consequentemente no custo (WAGHMARE et al., 2021).

A IRFD possui as mesmas etapas da liofilização: congelamento, secagem primária e secagem secundária. A diferença é que se acopla dentro da cuba do liofilizador um aquecedor com emissão de radiação infravermelha (IR) que irá fornecer energia para sublimação (LEE, 2021). IR fornece energia diretamente para a superfície do material e, portanto, causa seu rápido aquecimento gerando maior eficiência térmica e taxa de aquecimento mais rápida em comparação com o aquecimento convencional (ANTAL et al., 2017; WAGHMARE et al., 2021). Dessa forma, a IRFD é uma técnica de secagem que reúne as vantagens da liofilização, em termos de qualidade do produto, e da secagem por radiação infravermelha, reduzindo o tempo operacional e o consumo de energia (KRISHNAMURTHY et al., 2008; WAGHMARE et al., 2021).

Lin, Tsen e King (2005) foram os primeiros pesquisadores a estudarem a combinação da liofilização com aquecimento IR simultâneo para secagem de pedaços de batata doce. Para isso montaram um sistema, como esquematizado na Figura 5, que consistia em uma câmara de vácuo, condensador, bomba de vácuo e um radiador de cerâmica no infravermelho distante. As bandejas foram equipadas com arame para conter os materiais a serem secos no interior de uma câmara de secagem de aço inoxidável. As bandejas foram colocadas sob radiador de cerâmica e a operação de secagem por congelamento foi realizada sob vácuo a uma pressão absoluta de 0.3 mmHg. Os pesquisadores observaram uma economia no tempo variando de 16 a 58% ao utilizar o sistema combinado de liofilização com IR.

Em um segundo estudo, Lin et al. (2007) otimizaram a secagem por liofilização acoplada ao IR simultâneo utilizando o radiador de cerâmica com comprimento de onda distante para pedaços de inhame. Os pesquisadores obtiveram como resultado que o processamento de secagem ideal deve possuir distância entre a amostra e a placa FAR maior que 50 mm, temperatura de secagem entre 34–37 °C e espessura das fatias entre 7–8 mm para que se tenha menor diferença de cor, menor tempo de secagem e maior taxa de reidratação. Também observaram que a IRFD trouxe menor diferença de cor, bem como menor encolhimento devido à desidratação mais rápida, em comparação com a liofilização tradicional.

Figura 5 – Representação do liofilizador experimental com radiação infravermelha.

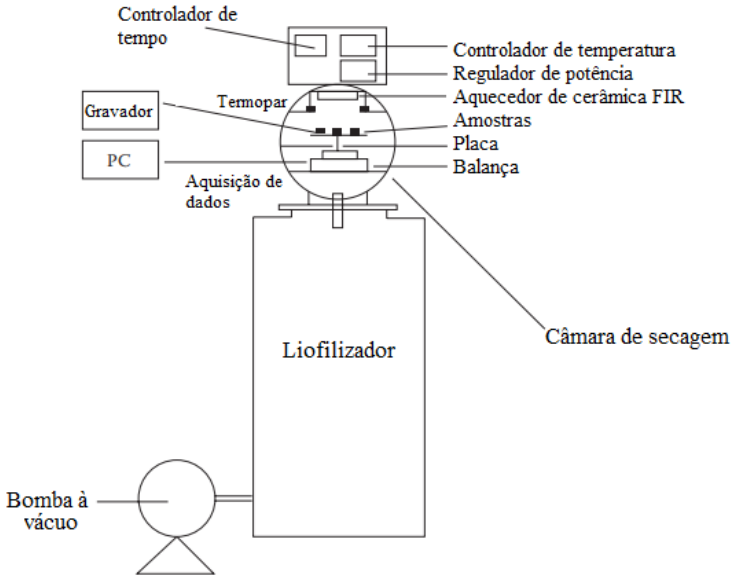

Fonte: Lin, Tsen e King (2005).

Khampakool, Soisungwan e Park (2019) investigaram a secagem por IRFD utilizando o comprimento de onda próximo em *snacks* de bananas com os seguintes ensaios: (1) liofilização tradicional, (2) liofilização com IR simultâneo na potência de 2.7 $kW \cdot m^{-2}$, (3) liofilização seguida por IR à 2.7 $kW \cdot m^{-2}$ quando as amostras obtiveram 20% de redução do peso e (4) liofilização com IR na potência inicial de 2.7 $kW \cdot m^{-2}$ e quando as amostras chegaram a 0 ºC aumentaram a potência para 4.0 $kW \cdot m^{-2}$. O ensaio (2) reduziu significativamente o tempo de secagem (213 min) em comparação com a liofilização tradicional (696 min), resultando em mais de 70% de economia de tempo e, todos os ensaios com IR melhoraram à crocância dos *snacks* de banana.

Wu, Zhang e Bhandari (2019) conduziram uma investigação experimental sobre a IRFD no comprimento de onda distante em cogumelo (*Cordyceps militaris*), sendo que a IRFD e a liofilização tradicional foram comparadas em diferentes temperaturas de secagem de 40, 50, 60 e 70 º C. Observou-se que o aumento da temperatura de secagem reduziu significativamente o tempo de secagem, bem como o consumo de energia para ambos os tratamentos. A IRFD reduziu até 17,78% do tempo de secagem e até 18,37% do consumo de energia na mesma temperatura de secagem em comparação com a liofilização tradicional. Os autores também concluíram que IRFD é uma técnica promissora para a aquisição de produtos desidratados de alta qualidade.

No estudo de Hnin et al. (2019) investigou-se a produção de iogurte seco com sabor de rosa por meio do uso de liofilização por infravermelho (IRFD). Nesta pesquisa, além do tempo

de processo também avaliou se a IRFD reduzia os compostos bioativos do iogurte e se havia diferença no sabor. Os resultados mostraram que a amostra seca por meio da IRFD e preparada a 55 °C recebeu a pontuação total mais alta entre todas as amostras. Porém, a secagem por IRFD reduziu ligeiramente o teor de fenólicos totais, antocianinas e flavonoides.

Além dos estudos já mencionados, muitos produtos alimentícios foram efetivamente secos por meio do processo combinado de liofilização por infravermelho, exibindo economia no tempo e gerando produtos com elevado valor agregado como, por exemplo, camarão tigre (CHAKRABORTY et al., 2011), iogurte de couve derretido (LAO et al., 2020), taro e batata frita (HNIN et al., 2019), sopa de cogumelo (LIU et al., 2020) e inseto comestível (KHAMPAKOOL et al., 2020).

Outros estudos também avaliaram a secagem por radiação infravermelha sequenciada por liofilização como no trabalho de Antal et al. (2017) com pêra. Porém, alguns estudos sugerem que a combinação da liofilização com a radiação infravermelho simultânea, a IRFD, é mais eficaz. Como por exemplo, no estudo de Wang, Zhang e Adhikari (2015) secando cogumelos *shiitake*, a combinação sequencial foi considerada inferior em comparação com a simultânea, uma vez que a primeira causou o colapso da estrutura celular na superfície e também produziu materiais com fraca capacidade de reidratação, enquanto que a combinação simultânea obteve um efeito significativo na retenção de aromas. Shih et al. (2013) também relataram as amostras de morango submetidas a secagem sequencial apresentaram uma menor taxa de reidratação que as amostras de morango apenas liofilizadas.

Apesar de vários estudos acoplando a liofilização com o aquecimento infravermelho ainda é necessário desenvolver a modelagem mecanicista de secagem com configuração experimental (KHAMPAKOOL; SOISUNGWAN; PARK, 2019) e otimizar parâmetros como faixas de comprimentos de ondas ideais para secagem de alimentos, tempo de atuação da radiação IR, altura da lâmpada e entre outros.

2.7 Radiação infravermelha

A radiação infravermelha (IR) é a parte do espectro eletromagnético que abrange os comprimentos de onda de 0,75 a 1.000 μm (SANDU, 1986), Figura 6. O efeito de aquecimento do Sol é predominantemente responsável pela radiação infravermelha, sendo caracterizada por ser uma das formas mais antigas de tratar os alimentos com calor, a qual os produtos alimentícios eram secos através da exposição da luz solar intensa, visando reduzir a atividade

de água e permitir períodos mais longos de armazenamento (RANJAN; IRUDAYARAJ; JUN, 2002).

O espectro da IR, Figura 6, é dividido em três categorias, nomeadamente IR próximo (NIR) (0,78–1,4 μm), IR médio (MIR) (1,4–3,0 μm) e IR distante (FAR) (3,0– 1000 μm) (RIADH et al., 2014; SANDU, 1986). Os emissores de ondas curtas, NIR, são os mais próximos do espectro visível e emitem raios infravermelhos com a temperatura do radiador correspondente em torno de 1300–2600 K. Este tipo de emissor é frequentemente considerado o mais poderoso porque pode atingir a temperatura máxima em poucos segundos. Emissores de infravermelho de onda média, MIR, emitem em temperaturas do radiador de 850–1200 K com tempo de resposta de cerca de um minuto. Os emissores de ondas médias são amplamente usados para secar e curar produtos alimentícios. Os emissores de ondas longas, FAR, têm a temperatura de radiação de 500–800 K. Este tipo de emissor leva mais de 5 minutos para atingir seu pico de potência emissiva. Emissores de ondas longas IR criam um fluxo de ar quente que é útil para processos que requerem uma combinação de convecção e aquecimento IR (DAS; DAS, 2010; RASTOGI, 2021).

Figura 6 – Espectros eletromagnético e localização da radiação infravermelha (IR).

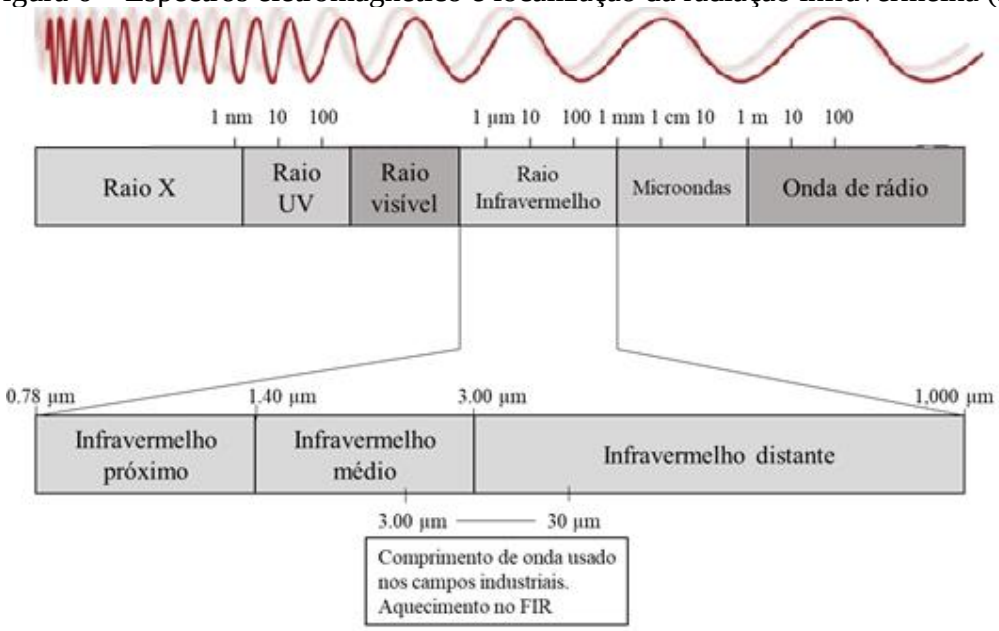

Fonte: Pan e Atungulu (2010).

A transferência de calor por IR ocorre sem contato direto com o matéria, sendo propagada como onda eletromagnética sem a requisição de um meio, portanto também pode se propagar em ambiente de vácuo (HUANG et al., 2021). As ondas ao atingirem o material podem

ser refletidas (ρ), absorvidas (α) ou transmitidas (τ). Se a transmissividade for infinitesimal, o material refletirá ou absorverá IR dependendo da natureza da radiação e das características da superfície do material, isso é chamado de emissividade (ε) e normalmente varia de 0 a 1. Os corpos negros absorvem toda a radiação que incide sobre eles e, portanto, têm emissividade de 1.0, em oposição a superfícies completamente refletivas (ε = 0) (PAN; ATUNGULU, 2010; RIADH et al., 2014).

O princípio da secagem de materiais por IR estabelece que, se o comprimento de onda da fonte de radiação coincide com o comprimento de onda de absorção do objeto irradiado (alimento), a substância absorve uma grande quantidade de energia infravermelha, alterando e agravando o movimento de suas moléculas, fazendo com que haja a transformação da radiação infravermelha em energia rotacional, causando o aquecimento da molécula e a evaporação da água. Neste processo o calor é transferido para o material a ser seco na forma de energia eletromagnética (PAN; ATUNGULU, 2010; PAWAR; PRATAPE, 2017).

Dessa forma, para o aquecimento das moléculas é necessário que o comprimento de onda irradiado seja o mesmo do comprimento de onda de absorção. Entretanto, alimentos são sistemas complexos com grandes moléculas bioquímicas, polímeros, sais inorgânicos e água. Assim, a maior absorção no espectro infravermelho é, geralmente, obtida pelas vibrações desses agregados moleculares (ou grupos estruturais moleculares) dentro de um fenômeno muito complexo de sobreposição recíproca. Para aminoácidos, proteínas e ácidos nucléicos os comprimentos de absorção correspondem a duas faixas: 3–4 μm e 6–9 μm. Enquanto lipídeos absorvem em três faixas do espectro: 3–4 μm, 6 μm e 9–10 μm. Açúcares, por sua vez, apresentam absorção em 3 μm e na faixa de 7 a 10 μm (SANDU, 1986).

A água possui picos de absorção de energia infravermelha nos comprimentos de onda em torno de 3,6; 12 e 15 μm, porém a gama entre 3,5-5,5 μm possui eficiência de secagem menor devido à baixa absortividade, como mostrado na Figura 7 (IL'YASOV; KRASNIKOV, 1991). As ligações O-H na água absorvem energia infravermelha e começam a girar com a mesma frequência da radiação incidente, essa transformação da radiação IR em energia rotacional causa a evaporação da água.

Figura 7 – Curva de absorção espectral de infravermelho para água.

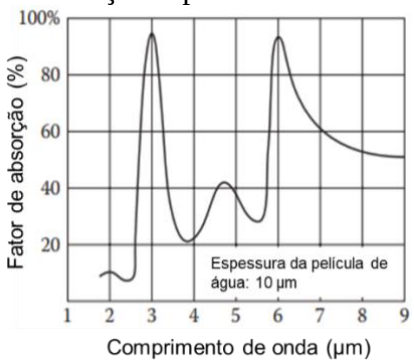

Fonte: Pan; Atungulu (2010).

A faixa espectral relativa à radiação térmica é distinta entre os especialistas. Para Sandu (1986) a região de interesse para alimentos é restrita a 0,75 a 15 µm, enquanto que Pan e Atungulu (2010) relataram que a faixa de 2,5 a 200 µm são mais comumente usados para secagem no IR.

Além do comprimento de onda da radiação, a profundidade de penetração da radiação também é um fator a ser considerado e, esta depende das características da amostra (por exemplo, o teor de água) e da espessura. Em comprimentos de onda próximo, a radiação infravermelha é transmitida através da água, enquanto no comprimento de onda distante é absorvida na superfície (SAKAI; HANZAWA, 1994). Portanto, a secagem de camadas finas parece ser mais eficiente na radiação infravermelha distante – FAR, enquanto a secagem de corpos mais espessos pode-se ter melhores resultados na radiação infravermelha próxima – NIR (NOWAK; LEWICKI, 2004).

Dessa forma, utilizando a uniformidade, espaçamento e espessura corretas, por exemplo, o aquecimento por radiação IR em alimentos oferece inúmeras vantagens, como maior eficiência energética, maior taxa e fluxo de transferência de calor, resultando em tempo reduzido de desidratação em relação ao método de secagem tradicional (RASTOGI, 2021). Estas vantagens podem ser explicadas por:

- O ar circundante entre a fonte de infravermelho e o produto não é aquecido e permanece à temperatura ambiente, tornando o processo eficiente em energia. Exceto quando o meio está saturado com vapor de água, pode ocorrer pouca absorção de energia infravermelha no produto (LEE, 2021; RASTOGI, 2021).

- As irregularidades da superfície não têm efeito significativo na taxa de transferência de calor durante o aquecimento infravermelho, o que resulta em um aquecimento mais uniforme (RASTOGI, 2021).
- Não é necessário contato direto com o material como ocorre na secagem por condução;
- A radiação infravermelha pode ser focada para aumentar a intensidade de aquecimento podendo ser projetada para atingir uma área específica, fornecendo assim tratamentos rápidos;
- Taxas de transferência de calor muito altas são possíveis com aquecedores compactos;
- Tempos de resposta rápidos (baixa inércia térmica) permitem um controle de processo fácil e rápido (PAN; ATUNGULU, 2010).

Devido às diversas vantagens, o aquecimento infravermelho foi adotado com sucesso para muitas operações unitárias no processamento de alimentos, ou seja, secagem, cozimento, torrefação, branqueamento, pasteurização e descongelamento, envolvendo o uso de geradores de radiação infravermelha, tais como lâmpadas elétricas especiais e painéis cerâmicos ou metálicos aquecidos por eletricidade ou gás (RATTI; MUJUMDAR, 2006; NINDO e MWITHIGA, 2011).

Como restrição da secagem por IR pode-se citar que a absorção total de energia no aquecimento infravermelho é limitada devido à incapacidade de penetrar mais profundamente no alimento. Assim, a energia IR é absorvida na superfície, o que permite que a camada externa seque mais rapidamente. Dessa forma, o aumento no volume da amostra impõe restrições à condução e, portanto, apenas uma pequena quantidade de energia total pode ser absorvida. Outra desvantagem é que o uso de aquecimento infravermelho para exposição prolongada de materiais biológicos pode causar rachaduras nos alimentos levando ao comprometimento da qualidade (LEE, 2021; RASTOGI, 2021).

Para a otimização da secagem de alimentos, ou seja a redução do tempo de secagem sem afetar significativamente a qualidade dos produtos, tem sido feitos estudos de aquecedores infravermelhos em conjunto com outros modos de aquecimento tradicionais (ar quente, à vácuo, liofilização), uma vez que o acoplamento da radiação infravermelha nos equipamentos de secagem é considerado como uma construção simples e fácil (RASTOGI, 2021). Ademais, a combinação diminui o tempo de processo e gera produtos secos com qualidade superior, devido à menor temperatura de secagem e menor nível de reações oxidativas (WU et al., 2007).

2.8 Problemas associados à secagem - Colapso

Mudanças indesejáveis nas propriedades físico-químicas e estruturais podem ocorrer durante a secagem de alimentos, afetando diretamente na qualidade do produto final. Dentre estas, pode-se citar a perda das características sensoriais, nutricionais e a estabilidade (KHALLOUFI; RATTI, 2003). No caso de produtos liofilizados, os principais parâmetros que influenciam a qualidade final são as taxas e temperatura de congelamento e temperatura de secagem (primária e secundária); bem como a pressão empregada no processo. Dessa forma, deve-se ter um controle das condições não apenas para encurtar o tempo de secagem, como também para evitar o derretimento e colapso do material (BERK, 2018).

O colapso é um fenômeno físico-químico que pode ser definido como fluxo viscoso que resulta de uma viscosidade reduzida acima da transição vítrea. O termo "colapso" tem sido usado para descrever a perda de estrutura, redução do tamanho dos poros e encolhimento volumétrico em alimentos secos (HARNKARNSUJARIT; CHAROENREIN, 2011). Devido à área de superfície reduzida, produtos colapsados possuem tempo de reconstituição prolongados durante a reidratação, menor solubilidade e endurecimento do produto (ANTAL et al., 2017). Outras desvantagens são perda de cor e aroma. (DURALLIU; MATEJTSCHUK; WILLIAMS, 2018).

A causa deste fenômeno está intimamente relacionada à transição vítrea. A temperatura de transição vítrea, T_g, é a temperatura à qual um sistema amorfo muda de estado vítreo para estado de borracha; sendo principalmente uma função do teor de água, peso molecular e natureza dos compostos de matéria seca em determinada substância (GENIN; RENÉ, 1995). Dessa forma, para um sistema de soluto que não cristaliza, mas permanece amorfo, a T_g geralmente é considerada a temperatura de colapso (T_c) (CHEN; OAKLEY, 1995). Determinar T_c é mais trabalhoso que T_g e, em geral, T_c é 1–2 ºC maior que T_g, o que significa que T_g pode ser usada como uma estimativa confiável para T_c (MERIVAARA et al., 2021).

Na secagem primária, quando o produto atinge temperaturas acima da T_c, observa-se perda de estrutura na região seca adjacente à interface gelo-vapor devido a uma transição vítrea no produto amorfo (MERIVAARA et al., 2021). Isto é, à medida que a temperatura aumenta, a viscosidade da fase amorfa do soluto diminui até que ocorra fluxo suficiente para resultar na perda da estrutura dos poros. Concomitante, a pressão interna do vapor de água causa fusão do gelo, e com isso, a água é removida por evaporação, ao invés da sublimação. Essa água descongelada plastifica a camada seca formada no início da secagem e a pressão interna

contribuiu para a formação de uma grande cavidade no interior da estrutura (HARNKARNSUJARIT; CHAROENREIN, 2011).

Durante a liofilização, a concentração do soluto da matriz aumenta progressivamente com a secagem (perda de água), o que faz com que a matriz se torne mais rígida e a T_g aumente. Assim, a temperatura na secagem secundária pode ser elevada, pois o gelo foi removido durante a secagem primária e o risco de derretimento ou colapso é mínimo (CHEN, 1995; MERIVAARA et al., 2021). O colapso normalmente será motivo de rejeição do produto devido ao aspecto indesejável (PIKAL; SHAH, 1990). Assim, para evitar problemas de qualidade durante a liofilização de um determinado produto, dois limites de temperatura mostraram-se essenciais: o núcleo congelado tem que estar abaixo da temperatura de início da fusão do gelo e a temperatura da matriz seca deve ser inferior à temperatura da T_g dos sólidos secos (KHALLOUFI; RATTI, 2003).

3 CONCLUSÃO

A IRFD é um método de secagem que reúne as vantagens da liofilização e da radiação infravermelha. Sendo assim, este método vem sendo desejado para aumentar a eficiência do processo de liofilização e gerar produtos com elevada qualidade. Neste novo método de secagem, o estudo do comprimento de onda aplicado é interessante para obter um processo de secagem otimizado, sem que ocorra o colapso, mantendo as características nutricionais e tecnológicas de produtos sensíveis ao calor. Dessa forma, será possível obter produtos com saudabilidade, praticidade e mais baratos em relação aos disponíveis no mercado.

REFERÊNCIAS

ANTAL, T. et al. Comparison of Drying and Quality Characteristics of Pear (Pyrus Communis L.) Using Mid-Infrared-Freeze Drying and Single Stage of Freeze Drying. **International Journal of Food Engineering**, v. 13, n. 4, p. 21, 2017.

ASSEGEHEGN, G. et al. Freeze-drying: A relevant unit operation in the manufacture of foods, nutritional products, and pharmaceuticals. **Advances in Food and Nutrition Research**, v. 93, p. 1–58, 2020.

BANSAL, A.; LALE, S.; GOYAL, M. Development of lyophilization cycle and effect of excipients on the stability of catalase during lyophilization. **International Journal of Pharmaceutical Investigation**, v. 1, n. 4, p. 214, 2012.

BERK, Z. Freeze drying (lyophilization) and freeze concentration. In: BERK, Z. (Ed.). . **Food Process Engineering and Technology**. [s.l.] Academic Press, 2009. p. 511–523.

BERK, Z. Freeze drying (lyophilization) and freeze concentration. **Food Process Engineering and Technology**, p. 567–581, 2018.

CHAKRABORTY, R. et al. Infrared-assisted freeze drying of tiger prawn: Parameter optimization and quality assessment. **Drying Technology**, v. 29, n. 5, p. 508–519, 2011.

CHEN, H. Functional Properties and Applications of Edible Films Made of Milk Proteins. **Journal of Dairy Science**, v. 78, n. 11, p. 2563–2583, 1995.

CHEN, T.; OAKLEY, D. M. Thermal analysis of proteins of pharmaceutical interest. **Thermochimica Acta**, v. 248, n. C, p. 229–244, 1995.

DAS, I.; DAS, S. K. Emitters and Infrared Heating System Design. In: PAN, Z.; ATUNGULU, G. G. (Eds.). . **Infrared Heating for Food and Agricultural Processing**. 1. ed. Boca Raton: Taylor & Francis Group, 2010. p. 57–88.

DURALLIU, A.; MATEJTSCHUK, P.; WILLIAMS, D. R. Humidity induced collapse in freeze dried cakes: A direct visualization study using DVS. **European Journal of Pharmaceutics and Biopharmaceutics**, v. 127, n. February, p. 29–36, 2018.

DUROUDIER, J.-P. Freeze-drying. In: JEAN-PAUL (Ed.). . **Heat Transfer in the Chemical, Food and Pharmaceutical Industries**. 1. ed. [s.l.] Elsevier, 2017. p. 359–377.

FAO. **Routledge handbook of religion and ecologyTHE STATE OF FOOD AND 2019 AGRICULTURE: MOVING FORWARD ON FOOD LOSS AND WASTE REDUCTION**. Rome: [s.n.].

FELLOWS, P. J. Freeze drying and freeze concentration. In: **Food Processing Technology Principles and Practice**. 3. ed. [s.l.] Woodhead Publishing Series, 2009. p. 687–699.

FELLOWS, P. J. Freeze drying and freeze concentration. **Food Processing Technology**, p. 929–945, 2017.

FERESHTEH, Z. **Freeze-drying technologies for 3D scaffold engineering**. [s.l.] Elsevier Ltd, 2018.

GARCIA-AMEZQUITA, L. E. et al. Freeze-drying: The Basic Process. **Encyclopedia of Food and Health**, p. 104–109, 2015.

GENIN, N.; RENÉ, F. Analyse du rôle de la transition vitreuse dans les procédés de conservation agroalimentaires. **Journal of Food Engineering**, v. 26, p. 391–408, 1995.

GEORGE, J. P.; DATTA, A. K. Development and validation of heat and mass transfer models for freeze-drying of vegetable slices. **Journal of Food Engineering**, v. 52, n. 1, p. 89–93, 2002.

HARNKARNSUJARIT, N.; CHAROENREIN, S. Influence of collapsed structure on stability of β-carotene in freeze-dried mangoes. **Food Research International**, v. 44, n. 10, p. 3188–3194, 2011.

HNIN, K. K. et al. Comparison of quality aspects and energy consumption of restructured taro and potato chips under three drying methods. **Journal of Food Process Engineering**, v. 42, n. 7, p. 1–13, 2019.

HUA, T.-C.; LIU, B.-L.; ZHANG, H. Heat-Mass Transfer Analyses and Modeling of the Drying Process. **Freeze-Drying of Pharmaceutical and Food Products**, p. 68–110, 2010.

HUANG, D. et al. Application of infrared radiation in the drying of food products. **Trends in Food Science and Technology**, v. 110, n. February, p. 765–777, 2021.

IL'YASOV, S. G.; KRASNIKOV, V. V. **PHYSICAL PRINCIPLES OF INFRARED ERADIATION OF FOODSTUFFS**. Nova Iorque: Hemisphere Publishing Corporation, 1991.

JESZKA-SKOWRON, M.; CZARCZYŃSKA-GOŚLIŃSKA, B. Chapter 21 - Raisins and the other dried fruits: Chemical profile and health benefits,. In: VICTOR R. PREEDY, R. R. W. (Ed.). . **The Mediterranean Diet**. Second Edi ed. [s.l.] Academic Press, 2020. p. 229–238.

KHALLOUFI, S.; RATTI, C. Quality deterioration of freeze-dried foods as explained by their glass transition temperature and internal structure. **Journal of Food Science**, v. 68, n. 3, p. 892–903, 2003.

KHAMPAKOOL, A. et al. Infrared assisted freeze-drying (IRAFD) to produce shelf-stable insect food from protaetia brevitarsis (white-spotted flower chafer) Larva. **Food Science of Animal Resources**, v. 40, n. 5, p. 813–830, 2020.

KHAMPAKOOL, A.; SOISUNGWAN, S.; PARK, S. H. Potential application of infrared assisted freeze drying (IRAFD) for banana snacks: Drying kinetics, energy consumption, and texture. **LWT - Food Science and Technology**, v. 99, n. October 2018, p. 355–363, 2019.

KRISHNAMURTHY, K. et al. Infrared Heating in Food Processing: An Overview. **COMPREHENSIVE REVIEWS IN FOOD SCIENCE AND FOOD SAFETY**, v. 7, p. 13, 2008.

KROKIDA, M. K.; PHILIPPOPOULOS, C. Volatility of apples during air and freeze drying. **Journal of Food Engineering**, v. 73, n. 2, p. 135–141, 2006.

LAO, Y. et al. Effect of combined infrared freeze drying and microwave vacuum drying on quality of kale yoghurt melts. **Drying Technology**, v. 38, n. 5–6, p. 621–633, 2020.

LEE, E. A Review on Applications of Infrared Heating for Food Processing in Comparison to Other Industries. In: **Innovative Food Processing Technologies: A Comprehensive Review**. Pohang: Elsevier, 2021. p. 1–25.

LIN, Y. P. et al. Dehydration of yam slices using FIR-assisted freeze drying. **Journal of Food Engineering**, v. 79, n. 4, p. 1295–1301, 2007.

LIN, Y. P.; TSEN, J. H.; KING, V. A. E. Effects of far-infrared radiation on the freeze-drying of sweet potato. **Journal of Food Engineering**, v. 68, n. 2, p. 249–255, 2005.

LIU, W. et al. A novel strategy for improving drying efficiency and quality of cream mushroom soup based on microwave pre-gelatinization and infrared freeze-drying. **Innovative Food Science and Emerging Technologies**, v. 66, n. September, p. 102516, 2020.

MERIVAARA, A. et al. Preservation of biomaterials and cells by freeze-drying: Change of paradigm. **Journal of Controlled Release**, v. 336, n. June, p. 480–498, 2021.

MORGAN, C. A. et al. Preservation of micro-organisms by drying; A review. **Journal of Microbiological Methods**, v. 66, n. 2, p. 183–193, 2006.

MUJUMDAR, A. S.; LAW, C. L.; WOO, M. W. **Freeze Drying: Effects on Sensory and Nutritional Properties**. 1. ed. [s.l.] Elsevier Ltd., 2015.

NINDO C.; MWITHIGA G., Infrared Drying. In: **Infrared Heating for Food and Agricultural Processing.** New York: CRC Press, 2011.

NOWAK, D.; LEWICKI, P. P. Infrared drying of apple slices. **Innovative Food Science and Emerging Technologies**, v. 5, n. 3, p. 353–360, 2004.

PAN, Z.; ATUNGULU, G. G. **Infrared Heating for food agricultural processing**. 1. ed. Boca Raton, FL: CRC Press, 2010.

PAWAR, S. B.; PRATAPE, V. M. Fundamentals of Infrared Heating and Its Application in Drying of Food Materials: A Review. **Journal of Food Process Engineering**, v. 40, n. 1, p. 1–15, 2017.

PIKAL, M. J. et al. The secondary drying stage of freeze drying: drying kinetics as a function of temperature and chamber pressure. **International Journal of Pharmaceutics**, v. 60, n. 3, p. 203–207, 1990.

PIKAL, M. J.; SHAH, S. The collapse temperature in freeze drying: Dependence on measurement methodology and rate of water removal from the glassy phase. **International Journal of Pharmaceutics**, v. 62, n. 2–3, p. 165–186, 1990.

PITTIA, P.; ANTONELLO, P. Safety by Control of Water Activity: Drying, Smoking, and Salt or Sugar Addition. In: PRAKASH, V. et al. (Eds.). . **Regulating Safety of Traditional and Ethnic Foods**. Academic P ed. [s.l.] Elsevier Inc., 2015. p. 7–28.

RAMBHATLA, S. et al. Heat and Mass Transfer Scale-up Issues during Freeze Drying: II. Control and Characterization of the Degree of Supercooling. **Aaps Pharmscitech**, v. 5, n. 4, p. 54–62, 2004.

RANJAN, R.; IRUDAYARAJ, J.; JUN, S. Simulation of infrared drying process. **Drying Technology**, v. 20, n. 2, p. 363–379, 2002.

RASTOGI, N. K. Infrared Heating in Drying Operations. In: **Innovative Food Processing Technologies: A Comprehensive Review**. Mysore: Elsevier, 2021. p. 1–21.

RATTI, C. Freeze drying for food powder production. In: **Handbook of Food Powders: Processes and Properties**. 1. ed. Canadá: Woodhead Publishing Limited, 2013. p. 57–84.

RATTI, C.; MUJUMDAR, A. S. Infrared Drying. In: **Handbook of Industrial Drying**. 3. ed. New York: CRC Press, 2006.

RIADH, M. H. et al. Infrared Heating in Food Drying: An Overview. **Drying Technology**, n. 3, p. 322–335, 2014.

SAGAR, V. R.; SURESH KUMAR, P. Recent advances in drying and dehydration of fruits and vegetables: A review. **Journal of Food Science and Technology**, v. 47, n. 1, p. 15–26, 2010.

SAKAI, N.; HANZAWA, T. Applications and advances in far-infrared heating in Japan. **Trends in Food Science and Technology**, v. 5, n. 11, p. 357–362, 1994.

SALEHI, F.; AGHAJANZADEH, S. Effect of dried fruits and vegetables powder on cakes quality: A review. **Trends in Food Science and Technology**, v. 95, n. August 2019, p. 162–172, 2020.

SALEHI, F.; KASHANINEJAD, M. Modeling of moisture loss kinetics and color changes in the surface of lemon slice during the combined infrared-vacuum drying. **Information Processing in Agriculture**, v. 5, n. 4, p. 516–523, 2018.

SANDU, C. Infrared Radiative Drying in Food Engineering: A Process Analysis. **Biotechnology Progress**, v. 2, n. 3, p. 109–119, 1986.

SHIH, C. et al. Sequential Infrared Radiation and Freeze-Drying Method for Producing Crispy Strawberries. **Transactions of the ASABE**, v. 51, n. 1, p. 205–216, 2013.

SVIECH, F.; UBBINK, J.; PRATA, A. S. Potential for the processing of Brazilian fruits - A review of approaches based on the state diagram. **LWT**, v. 156, p. 113013, 2022.

TANG, X.; PIKAL, M. J. Design of Freeze-Drying Processes for Pharmaceuticals: Practical Advice. **Pharmaceutical Research**, v. 21, n. 2, p. 191–200, 2004.

TECHNAVIO. **Freeze Dried Foods Market by Product and Geography - Forecast and Analysis 2021-2025**. Disponível em: <https://www.technavio.com/report/freeze-dried-foods-market-industry-analysis?v1=&utm_source=prnewswire&utm_medium=pressrelease&utm_campaign=TN-V2_rep1_wk52_001_22&utm_content=IRTNTR41477>. Acesso em: 21 jan. 2022.

WAGHMARE, R. B. et al. Recent Developments in Freeze Drying of Foods. In: **Innovative Food Processing Technologies**. Tamil Nadu: Elsevier, 2021. v. 3p. 82–99.

WANG, H. C.; ZHANG, M.; ADHIKARI, B. Drying of shiitake mushroom by combining freeze-drying and mid-infrared radiation. **Food and Bioproducts Processing**, v. 94, n. August, p. 507–517, 2015.

WU, L. et al. Vacuum drying characteristics of eggplants. **Journal of Food Engineering**, v. 83, n. 3, p. 422–429, 2007.

WU, X.; ZHANG, M.; BHANDARI, B. A novel infrared freeze drying (IRFD) technology to lower the energy consumption and keep the quality of Cordyceps militaris. **Innovative Food Science and Emerging Technologies**, v. 54, n. December 2018, p. 34–42, 2019.

XU, B. et al. Recent development in high quality drying of fruits and vegetables assisted by ultrasound: A review. **Food Research International**, v. 152, n. May 2021, 2022.

SEGUNDA PARTE
ARTIGO 1

Infrared-assisted freeze-drying (IRFD) of açai puree: Effects on the drying kinetics, microstructure, and bioactive compounds

Normas do periódico: Innovative Food Science and emerging technologies
ISSN: 1466-8564
(versão aceita)

Natália Leite Oliveira[a*], Sérgio Henrique Silva[a], Jayne de Abreu Figueiredo[a], Lais Bruno Norcino[a], Jaime Vilela de Resende[a]

[a] Universidade Federal de Lavras, Box 3037, 37200-000, Lavras, Minas Gerais, Brazil

*Corresponding author: Oliveira, N. L. Department of Food Science, Federal University of Lavras. E-mail address: natalia.oliveira1@estudante.ufla.br

Abstract

Comparison between near and far wavelength sections were evaluated in the infrared-assisted freeze-drying (IRFD) process of açai puree. Samples were dried using freeze drying (FD); near IRFD (NIRFD); far IRFD (FARFD); and infrared heating after 20% weight reduction, $NIRFD_{20\%WR}$ and $FARFD_{20\%WR}$. IRFD significantly reduced the total drying time, with NIRFD and FARFD taking 49.42% and 33.40% less time than FD, respectively. The structure of powdered using IRFD was more open and with larger pores. $FARFD_{20\%WR}$ had collapsed cells that compromised the functional properties of the powder (wettability, dispersibility). As for bioactive compounds, phenolic content was not affected by IRFD, ranging from 963.44 to 1025.60 mg/100 g. Antioxidant capacity increased (59.91 to 88.06%) when far infrared was used due to a Maillard reaction that generated antioxidant compounds and darker product. Content of anthocyanins reduced in samples dried by far infrared. Overall, NIRFD was more efficient, as it reduced total drying time without compromising product quality.

Industrial relevance: The high-energy consumption of traditional freeze-drying limit the large-scale industrial production of freeze-dried açai puree. The infrared-assisted freeze-drying has been contributions on reducing drying energy consumption with time saving varying from 24.73 to 49.42% compared to freeze-drying treatment, maintaining the color, apperance and nutritional quality of the açaí puree. Besides that, this study outstands that near wavelength lamps are more suitable for food drying by IRFD.

Keywords: Anthocyanin; Collapse**;** Energy consumption; Phenolic; Quality; Wettability

1. Introduction

Açai (*Euterpe oleracea* Martius) is a native fruit of Northern Brazil that has been consumed since ancient times by the indigenous people (Schauss et al., 2006; Vasconcelos et al., 2019). Currently, açai consumption around the world is expanding, and analysts suggest the market is expected to grow by US$ 317.55 million during 2021–2025 (TechNavio, 2021). This is due to a range of therapeutic and healthpromoting benefits, including its extraordinary antioxidant and antiinflammatory properties when compared to other fruits (Silva et al., 2019; Heinrich, Dhanji, & Casselman, 2011). The health benefits provided by this Brazilian fruit are associated with its phytochemical composition rich in polyphenols such as anthocyanins and flavonoids (Pacheco-Palencia, Duncan, & Talcott, 2009). However, fresh açai is highly perishable, degrading quickly due to high microbial load, enzyme activity and high temperature and humidity in production areas (Pavan, Schmidt, & Feng, 2012). Furthermore, polyphenols are highly unstable during storage and processing (Pacheco-Palencia et al., 2009). To get around this problem, freeze-drying is an option (Oliveira et al., 2020).

Freeze-drying is a process based on the removal of water by sublimation, in which the product is first frozen (90% reabsorption of moisture), as it produces a porous and friable structure (Berk, 2018; Fellows, 2009; Oliveira et al., 2020; Ratti, 2013). These features are achieved due to the low temperatures used during the process. Although freeze-drying is a wellaccepted process, it is expensive when compared to other drying methods, as it has high energy consumption due to its long drying time (Berk, 2018; Fellows, 2009; Waghmare, Perumal, Moses, & Anandharamakrishnan, 2021). To overcome the shortcomings of freeze-drying, a promising method is to combine it with infrared (IR) radiation heating (Antal, Tarek-Tilistyák, Cziáky, & Sinka, 2017; Hnin, Zhang, Li, & Wang, 2019; Khampakool, Soisungwan, & Park, 2019; Liu, Zhang, Adhikari, & Chen, 2020; Pan & Atungulu, 2010; Pawar & Pratape, 2017; Salehi & Kashaninejad, 2018; Shih, Pan, McHugh, Wood, & Hirschberg, 2013; Wang, Zhang, & Adhikari, 2015; Wu et al., 2019).

Infrared radiation is the part of the electromagnetic spectrum that is predominantly responsible for the solar heating effect, covering a wavelength range between 0.75 and 1000 μm (Pawar & Pratape, 2017). IR is divided into near infrared (NIR), mid infrared (MIR), and far infrared (FAR), corresponding to spectral ranges of 0.75–3.0, 3.0–25, and 25–1000 μm, respectively (Pan & Atungulu, 2010). Some authors claim that drying thicker products is more efficient when using NIR, while FAR yields better results when drying thin layers (Riadh,

Ahmad, Marhaban, & Soh, 2014). Wang et al. (2015) studied the combination of freeze-drying and MIR and also observed a reduction in drying time and improved aroma preservation of the studied product.

During the infrared-assisted freeze-drying (IRFD) process, the energy needed for water sublimation is provided by the IR instead of the electric heating plate, which increases heat transfer rates (Pan & Atungulu, 2010). Several studies have shown IR reduced freeze-drying time by up to 48% without compromising the quality of several products such as banana snacks; slices of lemon, strawberry, apple, and pear; shiitake mushrooms; potato and taro chips; among others (Antal et al., 2017; Antal & Kerekes, 2016; Hnin, Zhang, Li, & Wang, 2019; Khampakool et al., 2019; Liu et al., 2020; Salehi & Kashaninejad, 2018; Shih et al., 2013; Wang et al., 2015; Wu, Zhang, & Bhandari, 2019). However, none has analyzed the influence of IR wavelength on the properties of the final product.

Therefore, the object of this work was to evaluate the effects of NIR and FAR-assisted freeze-drying on the drying time, the energy consumption, the microstructural characteristics and the preservation of the physicochemical and chemical characteristics of freeze-dried açai puree.

2. Materials and methods

2.1 Materials and characterization of açaí pulp

Açai puree was obtained from stores in Belo Horizonte, State of Minas Gerais, Brazil and was characterized by proximate composition (moisture, lipid, total carbohydrates, protein and ash) following the standard method AOAC (2006).

2.2 Infrared freeze-drying system

A drying chamber connected to a L4KR freeze-dryer (Edwards, São Paulo, Brazil) was built to install the infrared, temperature and sample weight sensors (Figure 1). The freeze-dryer consisted of a vacuum drying chamber, condenser at -40ºC, vacuum pump at 99.8 Pa, infrared lamp, temperature controller (thermostat), and weight and temperature (type T thermocouples) sensors. Infrared lamps were attached to the top of the drying chamber, 20 cm from the sample. Two types of IR lamps providing 2.0 W/m² of heat intensity were used: near infrared (NIR) (150-Watt, TheraBulb, China) and far infrared (FAR) (150-Watt, Heating, China). The

temperature inside the chamber was measured using a Type T thermocouple located 25 cm from the IR lamp and coupled to a thermostat (Import WEB, W3001). Temperature was set between 32 to 35ºC and controlled by the thermostat switching the IR lamp on and off. To monitor weight reduction, the samples were placed on a scale also coupled to the data acquisition system.

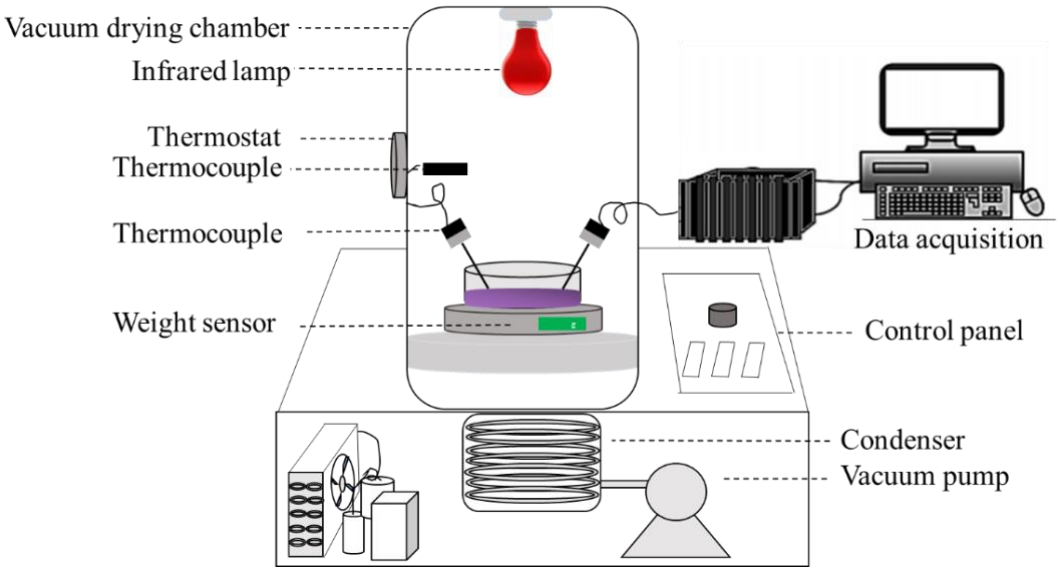

Figure 1 – Infrared-assisted freeze-dryer

2.3 Drying process (freeze-drying and infrared radiation)

Samples of approximately 200 g of açai puree for each treatment were stored in 500 mL plastic pots (12 cm in diameter and 5 cm in height), reaching a 2 cm thickness. Samples were frozen at -75 °C (Coldlab, CL120-86V, Piracicaba, Brazil) and dried in freeze-dryer (L4KR, Edwards, São Paulo, Brazil). Powdered products were removed from the freeze-dryer, hermetically packed into identified polyethylene bags, and stored in desiccators containing silica gel until analysis.

2.3.1 Monitoring of mass and temperature

Temperature was measured during the freeze-drying process using Type T thermocouples (Copper-Constantan), 1.5 mm in diameter and 100 mm in length. Data were recorded at 5 min intervals using a signal conditioning system (SCXI-1000, National

Instruments Corporation, Budapest, Hungary) using LabView 8.5 software (National Instruments Corporation, Newbury, Ireland). Temperature variation of the samples was measured using three Type T thermocouples.

To determine weight reduction, weights were measured every 2.5 min by a scale coupled to a data acquisition system. Trials were carried out until the moisture content in samples reached < 8.0%.

2.4 Experimental design

Infrared-assisted freeze-drying trials were setup in a completely randomized design (CRD) with five treatments: 1) freeze-drying control treatment, FD; 2) freeze-drying + continuous near infrared radiation heating, NIRFD; 3) freeze-drying + near infrared radiation heating after 20% weight reduction, $NIRFD_{20\%WR}$; 4) freeze-drying + continuous far infrared radiation heating, FARFD; 5) freeze-drying + far infrared radiation heating after 20% weight reduction, $FARFD_{20\%WR}$.

2.5 Drying process
2.5.1 Radiant energy

The amount of radiant energy was calculated according to Khampakool et al. (2019). IR lamp provided the radiant energy on the frozen samples, working as a driving force of sublimation under vacuum. Total energy (E_T) required to sublime ice is given by Equation 1:

$$E_T = E_{VC} + E_{RD} \quad (1)$$

where E_T is total energy (kJ), E_{VC} is vacuum energy (kJ), and E_{RD} is radiant energy (kJ).

The total energy required to sublime the ice from initial moisture content (M_0) to final moisture content (M_f) is shown in Equation 2:

$$E_T = m \times (M_0 - M_f) \times L_S \quad (2)$$

where m is the sample mass (kg) and L_s is the latent heat for ice sublimation (L_s = 2.834 x 10^3 $kJ \cdot kg^{-1}$).

For FD, E_T was considered equal to E_{VC}. For IRFD treatments, vacuum energy ($E_{VC,IRFD}$) was calculated as the ratio of IRFD drying time (t_{IRFD}) to FD drying time (t_{FD}), as shown in Equation 3:

$$E_{VC,IRFD} = E_T \times \frac{t_{IRFD}}{t_{FD}} \quad (3)$$

where $E_{VC,IRFD}$ is IRFD vacuum energy (kJ), t_{IRFD} is IRFD drying time (min), and t_{FD} is FD time (min).

2.5.2 Drying kinetics

The drying kinetics of the treatments was measured through mass reduction during the freeze-drying process. Drying curves were obtained as a function of moisture ratio (*MR*) over time, using Equation 4:

$$MR = {}^{u}/_{u_o} \quad (4)$$

where u is the water content during the drying process (g H_2O/g dry matter) and u_o is the initial water content (g H_2O/g dry matter).

The logarithmic (Equation 5), diffusion approximation (Equation 6) and Newton (Equation 7) models were fitted to select the model that best describes the drying curve of the samples in each treatment. These models have been used to characterize drying kinetics of foods (Antal et al., 2017; Doymaz, 2014; Ilter et al., 2018; Salehi & Kashaninejad, 2018; Wu, Orikasa, Ogawa, & Tagawa, 2007).

$$MR = a \cdot exp(-K \cdot t) + c \quad (5)$$

$$MR = a \cdot exp(-K \cdot t) + (1 + a)exp(-K \cdot b \cdot t) \quad (6)$$

$$MR = exp\ (-K \cdot t) \quad (7)$$

Where *MR* is the moisture ratio, *K* is the drying constant (h^{-1}), *t* is the time (h), and *a*, *b*, *c* are constants determined by the experimental data.

The coefficient of determination (R^2) and the root mean square error (RMSE) were calculated to evaluate the goodness-of-fit of the models. The highest values of R^2 and the lowest values of RMSE were chosen for the fit.

2.6 Evaluation of the characteristics of freeze-dried açai puree
2.6.1 Scanning electron microscopy (SEM)

Micrographs of the surface of freeze-dried açai puree samples cut in the radial direction were taken with 100 × magnification using a scanning electron microscope (Leo 1430 VP, Zeiss, Cambridge, UK) with an accelerating voltage of 20 kV. Samples were fixed to stubs using double-sided tape, then sputter-coated with gold at 200 A for 180 s prior to micrography.

2.6.2 Collapse

Collapse measurements were made visually using macrographs taken prior and after the freeze-drying and infrared-assisted freeze-drying processes. For this, a support was designed so that macrographs were recorded at the same location, distance, height and position in relation to the samples.

2.6.3 Water activity (a_w)

Water activity (a_w) was measured at 25ºC ± 1ºC using a dew-point hygrometer (3TE, Aqualab - Decagon, Washington, USA).

2.6.4 Color

The color of the samples was measured with a colorimeter (CR-5, Konica Minolta Sensing Inc., Sakai, Japan) using a cylindrical coordinate system that includes L*, a*, b*, and hue angle (h°). L* indicates lightness and ranges from 0 (black) to 100 (white), whereas a* ranges from green to red (-a*, green; +a*, red) and b* ranges from blue to yellow (-b*, blue; +b*, yellow). Hue angle (h°) is defined as starting at the +a* axis and is expressed in degrees: 0° would be +a* (red), 90° would be +b* (yellow), 180° would be -a* (green), and 270° would be -b* (blue).

2.7 Bioactive Compounds
2.7.1 Anthocyanin content

Total anthocyanin content was determined by the pH differential method, following the methodology by AOAC (2006). Around 0.5 (± 0.01) g of each sample was diluted in two buffer solutions (pH 1 and 4.5) and absorbance was measured at 520 and 700 nm in an UV/Visible spectrophotometer (Cary 50, Varian, Palo Alto, CA), with four technical replicates. Results were expressed in mg cyanidin-3-glucoside/100 g of lyophilized powder sample.

2.7.2 Total phenolic content

Total phenols were determined according to the Folin-Ciocalteu spectrophotometric method, described in Singleton and Rossi (1965) and used by Türkyılmaz, Tagı, Dereli, and Ozkan (2013). Absorbance of 0.5 ± 0.01 g of each sample was measured in an UV/Visible spectrophotometer (Cary 50, Varian, Palo Alto, CA) with four technical replicates. Phenolic content was calculated based on a standard gallic acid curve and was initially expressed as mg gallic acid equivalent (GAE) per lyophilized powder sample.

2.7.3 Antioxidant capacity

The measurement of stable free radical 1,1-diphenyl-2-picrylhydrazyl (DPPH) was performed according to the methodology of BrandWilliams, Cuvelier, and Berset (1995) and used by Arend et al. (2017). Absorbance of 0.5 ± 0.01 g of each sample was measured in an UV/ Visible spectrophotometer (Cary 50, Varian, Palo Alto, CA) with four technical replicates. Results were expressed as percentage.

2.8 Functional properties

To evaluate the functional properties, samples were ground with mortar and pestle and the particle size was homogenized by passing them through a sieve with an opening size between 0.250 and 0.84 mm.

2.8.1 Bulk density

For bulk density, 2 g of powdered samples were transferred to a 10 mL graduated cylinder and vibrated for 1 min. Bulk density was calculated by dividing the mass (g) of the powder by the volume (mL) occupied in the cylinder.

2.8.2 Wettability

For wettability, 5 g of powdered samples was suspended on the surface of 100 mL of water at 20 °C in a beaker with an internal diameter of 80 mm. The time required for the powder to sink and disappear from the surface of the water, known as the wetting time, was measured using a stopwatch.

2.8.3 Dispersibility

Dispersibility was measured with a methodology proposed by the Brazilian Ministry of Agriculture, Livestock, and Food Supply (Brasil, 2006) with adaptations. A total of 5 g of each sample was manually shaken in 100 mL of water at 25 ◦C and part of the mixture was filtered with filter paper. The resulting filtrate was oven-dried (Sterilifer, SX 1.2 DTME, Brazil) at 105 °C until constant weight and dry matter content was determined. Dispersibility (*DS*) was calculated with Equation 8:

$$DS = \frac{(w + a)S_P}{a \cdot S_j} \times 100 \quad (8)$$

where *w* is the water mass (g), *a* is the sample mass (g), *Sp* is the total solids content in the powder and *Sj* is the dry matter of the reconstituted sample.

2.8.4 Water Absorption Capacity (WAC)

Water absorption capacity (WAC) was determined using the centrifugal method. First, 0.1 g of sample was suspended in 10 mL of distilled water. The suspension was incubated at room temperature for 30 min, centrifuged at 2100×G for 30 min, and the supernatant was

collected and measured in a 10 mL graduated cylinder. The water absorption capacity (g/g) was calculated using Equation 9:

$$WAC = \frac{(V_I - V_F)}{m} x\ \rho_{water} \quad (9)$$

where V_I and V_F are the initial and final volumes of the solution, respectively, m is the initial mass of the sample and ρ_{water} is the density of water.

2.9 Statistical analysis

The results of the chemical and physicochemical analyzes were subjected to analysis of variance (ANOVA) with a significance level of 0.05. When ANOVA was significant, multiple comparisons between treatments were performed using Tukey's post hoc test (p<0.05). Statistical tests and modeling of the drying curves were performed using Statistica® 8.0 Software (StatSoft, Tulsa, USA).

3. Results and discussion

3.1 Characterization of açaí pulp

The açai puree used in this study had moisture of 94.65 ± 0.10%, lipid content of 45.45 ± 0.53%, total carbohydrates and fibers of 29.53 ± 3.16%, protein content of 13.69 ± 0.55%, and mineral content of 5.97 ± 2.09%. Costa, Silva, and Vieira (2018) and Tonon, Alexandre, Hubinger, and Cunha (2009) found similar results for lipids, carbohydrates, and ash, but different values for protein and moisture content, which can be explained by factors such as harvest season, ripeness and size of fruits, climate and processing conditions (Cohen et al., 2007).

3.2 Monitoring of mass and temperature during FD and IRFD

Figure 2a shows the temperature profiles of all treatments during the freeze-drying process. Samples had a temperature between -50 and -40ºC at the first reading, then were quickly heated to temperatures close to -10ºC. After this, the primary and secondary drying steps are identified.

During the primary drying step, water removal occurs by sublimation and the temperature remains constant, as all heat is used for the phase change (heat of sublimation) (Hua, Liu, & Zhang, 2010). Primary drying mainly occurred at temperatures between -10 and 13ºC, depending on the treatment, Figure 2a. During the secondary drying step, water is removed by desorption and the temperature of the product significantly increases, reaching 30 to 40ºC at the end of drying, Figure 2a. Both steps can occur at the same time, as the secondary drying can start before the complete removal of ice. In this situation, the sublimating ice keeps the food temperature under control. When the ice is completely sublimated, an increase in temperature occurs; this point signals the end of the primary drying (Gonçalves et al., 2018; Orrego, 2008).

The control treatment (FD) had the longest primary drying (45 h), while infrared radiation drastically reduced this period: 32 h for $FARFD_{20\%WR}$, 27 h for FARFD, 10 h for $NIRFD_{20\%WR}$, and 13 h for NIRFD. In IRFD treatments, the açai puree directly absorbed infrared energy in the form of electromagnetic waves, increasing the temperature in the center of the samples. As a consequence, there was an increase in the average drying rate, a faster removal of ice crystals, and a shorter primary drying time (Antal et al., 2017). Combined infrared radiation and freeze-drying also shortened the primary drying step in banana snacks, using short-wave IR, (Khampakool et al., 2019), pear (L.) slices using mid-wave IR (Antal et al., 2017), *Cordyceps militaris* and yam slices, using long-wave IR (Lin, Lee, Tsen, & King, 2007; Wu et al., 2019).

Far-infrared treatments had a longer primary drying compared to treatments with near-infrared radiation. According to Krishnamurthy, Khurana, Jun, Irudayaraj, and Demirci (2008), both the penetration capacity and the reflection of IR radiation increase as the radiation wavelength decreases, meaning NIR has a greater penetration capacity than FAR. Hashimoto, Oshita, Yamazaki, and Shimizu (1994) studied the penetration of FAR energy into sweet potato and found it reached depths between 0.26 and 0.36 mm below the surface, while NIR radiation penetrated around 0.38 to 2.54 mm. In addition to the wavelength, the composition and structure of the product determine IR radiation penetration (Rastogi, 2021).

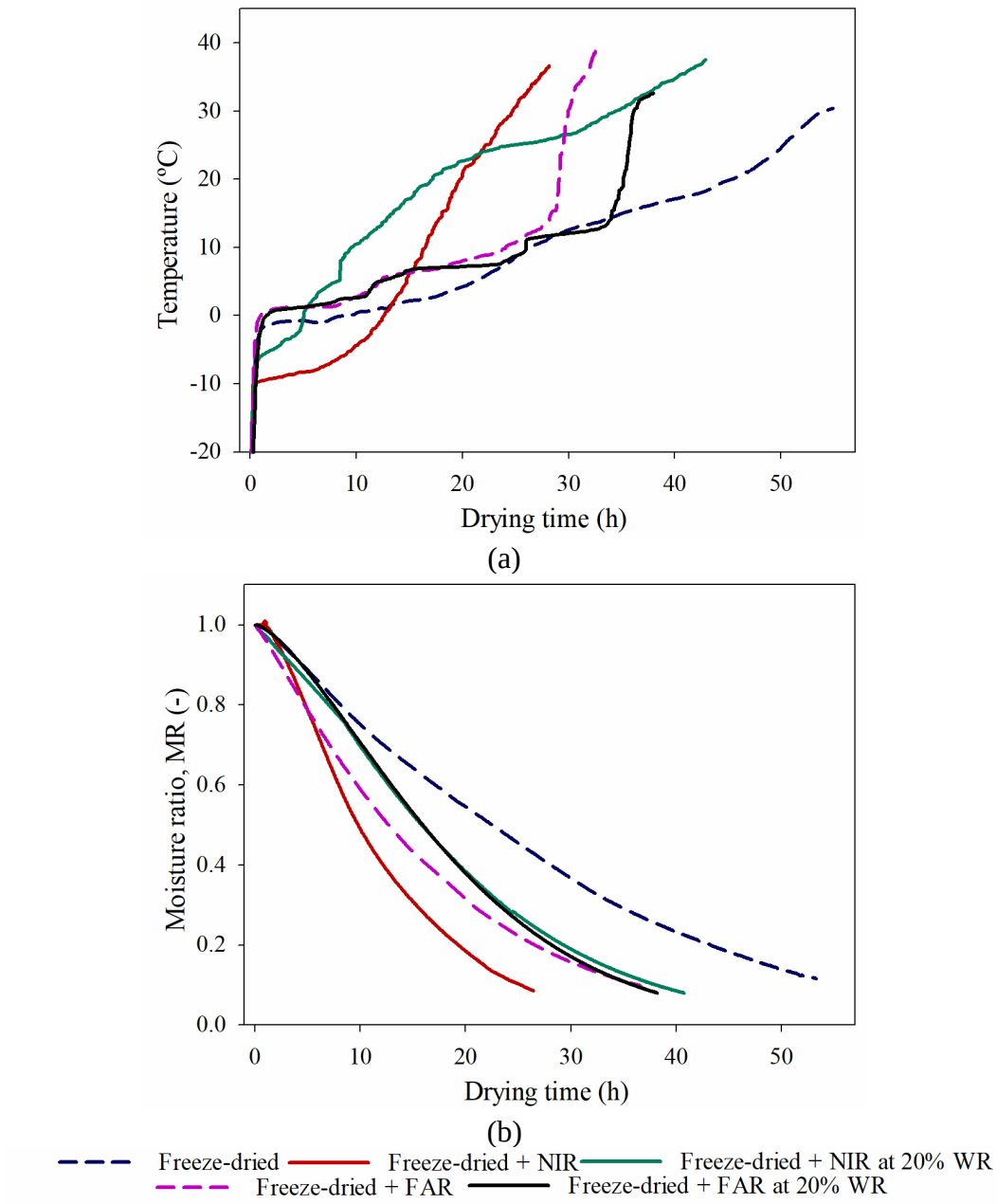

Figure 2 – (a) Temperature profile and (b) moisture ratio of açai puree samples during freeze-drying (FD) and freeze-drying + near (NIR) or far (FAR) infrared radiation. Infrared radiation was either applied continuously or after 20% weight reduction (20%WR).

Moisture loss was affected by treatments (Figure 2b). Table 1 shows that infrared-assisted freeze-drying treatments had significantly lower total drying times compared to conventional FD. FD had a drying time of 53.72 h, while the total drying time for NIRFD and FARFD were 27.17 h (a time saving of 49.42%) and 35.78 h (33.40%), respectively. Whereas the average drying rate increased from 3.72 g/h in the FD treatment to 5.59 and 7.36 in FARFD and NIRFD treatments, respectively (Table 1). Infrared radiation under vacuum condition

increases mass transfer, and this combination has great potential for fast drying at low temperatures (Khampakool et al., 2019; Salehi & Kashaninejad, 2018).

Table 1 – Total drying time, average drying rate, time saving, vacuum energy, and radiant energy of freeze-drying (FD), near-infrared-assisted freeze-drying (NIRFD), freeze-drying + near-infrared heating after 20% weight reduction ($NIRFD_{20\%WR}$), far-infrared-assisted freeze-drying (FARFD) and, freeze-drying + far-infrared heating after 20% weight reduction ($FARFD_{20\%WR}$).

	Total drying time (h)	Average drying rate (g/h)	Time saving (%)	Vacuum energy (kJ)	Radiant energy (kJ)
FD	53.72 ± 0.38^{a}	3.72 ± 0.02^{a}	-	192.71 ± 0^{a}	-
NIRFD	27.17 ± 0.82^{b}	7.36 ± 0.22^{b}	49.42 ± 1.24^{a}	93.98 ± 5.45^{b}	98.74 ± 5.45^{a}
$NIRFD_{20\%WR}$	40.43 ± 0.38^{c}	4.94 ± 0.04^{c}	24.73 ± 1.19^{b}	146.91 ± 3.72^{c}	45.80 ± 3.71^{b}
FARFD	35.78 ± 0.96^{d}	5.59 ± 0.15^{d}	33.39 ± 2.21^{c}	130.85 ± 2.73^{d}	61.86 ± 2.73^{c}
$FARFD_{20\%WR}$	37.50 ± 0.50^{d}	5.33 ± 0.07^{cd}	30.19 ± 1.40^{c}	136.21 ± 1.03^{d}	56.50 ± 1.03^{c}

Note: Values correspond to the mean and standard deviation. Means followed by the same letter do not differ according to Tukey's post-hoc test ($p<0.05$).

For $NIRFD_{20\% WR}$ and $FARFD_{20\% WR}$, infrared radiation heating began 8 hours after the start of the freeze-drying process, resulting in a decline in the average drying rate compared to treatments using continuous IR (average drying rates were 4.94 g/h for $NIRFD_{20\%WR}$ and 5.33 g/h for $FARFD_{20\%WR}$), Table 1. Despite the reduction in the moisture ratio, both treatments had lower total drying time compared to FD, with time savings of 24.74 and 30.20% for $NIRFD_{20\% WR}$ and $FARFD_{20\% WR}$, respectively.

NIRFD proved to be more effective for rapid production of freeze-dried high-value food products. However, for treatments where infrared radiation started after 20% weight reduction, FAR was more efficient than NIR. After this period there was a reduction in the thickness of the product and both lamps reached the same penetration depth. According Bi et al. (2014), far infrared (4–100 μm) is absorbed on the surface of materials and is suitable for drying thin layers, while medium and near infrared (0,75–4 μm) is characterized by higher radiation frequency and greater penetration depth, causing adaptability of thicker agricultural samples, such as the açaí puree thickness at the beginning of drying. Furthermore, FAR radiation has wavelengths compatible with the infrared energy absorption peaks of water. Thus, the -OH bonds of water absorb more infrared energy in the long wavelength and begin to rotate with the same frequency as the incident radiation. This transformation of IR radiation into rotational energy causes water evaporation (Das & Das, 2010; Pawar & Pratape, 2017).

3.3 Radiant energy

The total energy required to dry acai puree was 192 kJ. In freeze-drying (FD) treatment, the total energy corresponds only to vacuum energy (192 kJ), which is the energy needed to supply the ice sublimation heat (vacuum energy), Table 1. In the freeze-drying process, among the freezing, sublimation, water vapor condensation and vacuum maintenance steps, sublimation is the one that consumes the most energy (Khampakool et al., 2019). In treatments using IR, the total energy (192.7 kJ) is the sum of vacuum energy and radiant energy (supplied by the lamp). The radiant energy provides the driving force for the sublimation of ice and subsequent rapid drying. Thus, by coupling infrared radiation to the freeze-drying process, the vacuum energy decreased, for example to 93.98 kJ for NIRFD and 136.21 kJ for $NIRFD_{20\%WR}$, Table 1.

3.4 Drying kinetics

Table 2 shows the estimated coefficients for the logarithmic, diffusion approximation and Newton models. All models had a good fit to açai puree drying data, since R^2 values ranged from 0.975 to 0.999 and RMSE values were low, ranging from 0.002 to 0.069.

FD had the lowest drying constant, *K*, among treatments (0.024, 0.061 and 0.033 h^{-1} for the logarithmic, diffusion approximation and Newton models, respectively), corresponding to its slower average drying rate (3.72 g/h). In treatments using infrared radiation, *K* values increased, indicating a faster drying process (Lin, Tsen, & King, 2005). The highest value for *K* was found for NIRFD (0.059 h^{-1}, 0.439 h^{-1} and 0.073 h^{-1} for the logarithmic, diffusion approximation and Newton models, respectively), in agreement to the values of average drying rate. $NIRFD_{20\%WR}$ and $FARFD_{20\%WR}$ had lower *K* values compared to NIRFD and FARFD, attributed to the slower average drying rate in the initial stage without infrared radiation.

Table 2 – Coefficients and goodness-of-fit of the logarithmic, diffusion approximation, and Newtonian models for açai puree drying subjected to freeze-drying (FD), near-infrared-assisted freeze-drying (NIRFD), freeze-drying + near-infrared heating after 20% weight reduction ($NIRFD_{20\%WR}$), far-infrared-assisted freeze-drying (FARFD) and, freeze-drying + far-infrared heating after 20% weight reduction ($FARFD_{20\%WR}$).

	Logarithmic Model $MR = a \cdot \exp(-K \cdot t) + c$					Diffusion approximation $MR = a \cdot \exp(-K \cdot t) + (1 + a)exp(-kbt)$					Newton model $MR = \exp(-K \cdot t)$		
	a	*K* (h^{-1})	*c*	R^2	RMSE	*a*	*K* (h^{-1})	*b*	R^2	RMSE	*K* (s^{-1})	R^2	RSME
FD	1.277	0.024	-0.251	0.999	0.026	-11.78	0.061	0.948	0.999	0.034	0.033	0.992	0.015
NIRFD	1.319	0.059	-0.224	0.997	0.02	-0.355	0.439	0.227	0.999	0.004	0.073	0.98	0.056
$NIRFD_{20\%WR}$	1.492	0.028	-0.449	0.998	0.016	-2.317	0.11	0.744	0.999	0.005	0.047	0.983	0.051
FARFD	1.173	0.048	-0.136	0.998	0.016	-0.195	0.283	0.246	0.998	0.016	0.056	0.992	0.034
$FARFD_{20\%WR}$	1.508	0.029	-0.434	0.997	0.023	-3.117	0.116	0.772	0.999	0.002	0.048	0.975	0.069

a, *b*, *c*: constants determined by the experimental data. *K*: drying constant (s^{-1}). R^2: coefficient of determination. RMSE: root mean square error

3.5 Analysis of freeze-dried açai puree
3.5.1 SEM

The structure of the powdered açai puree under different drying treatments was observed under a scanning electron microscope (Figure 3). The açai puree obtained by FD had a microstructure with several small pores (Figure 3a). This resulted from the drying front moving from the center to the surface of the sample with a slow and constant speed, causing minimal changes in the açai puree structure during drying (Jiang, Zhang, Mujumdar, & Lim, 2013; Khampakool et al., 2019; Shih et al., 2013).

IRFD samples (Figure 3b, 3c, 3d, 3e) had less compact structures with larger pores, especially in samples subjected to continuous IR (NIRFD, Figure 3b; and FARFD, Figure 3d), which is attributed to the internal vaporization caused by IR radiation. The sample dried by $NIRFD_{20\%WR}$ (Figure 3c) had large pores in the center and collapsed structures, while the açai powder submitted to $FARFD_{20\%WR}$ (Figure 3e) had a dense surface layer or crust and also collapsed structures.

Similar results using FD and IRFD were obtained by Hnin, Zhang, Devahastin, and Wang (2019), Khampakool, Soisungwan, You, and Park (2020) and Pan, Shih, McHugh, and Hirschberg (2008) in studies with yogurt and freeze-dried bananas. The authors reported that the use of IR during freeze-drying promotes the instantaneous heating of water molecules and the generated water vapor expands cell walls, resulting in larger pores in the products (Shih et al., 2013). There was no difference between the structures of NIR- and FAR-assisted freeze-dried products.

3.5.2 Collapse

Figure 3 also shows the macrographs of powdered açai puree submitted to different drying treatments. Samples dried by IRFD were slightly darker than FD samples. Samples using FAR radiation heating (FARFD and $FARFD_{20\%WR}$) were more compact and rigid. In addition, the $FARFD_{20\%WR}$ sample was collapsed after treatment, attributed to the thawing of the açai puree during drying. Samples using NIR radiation had a soft appearance, similar to FD.

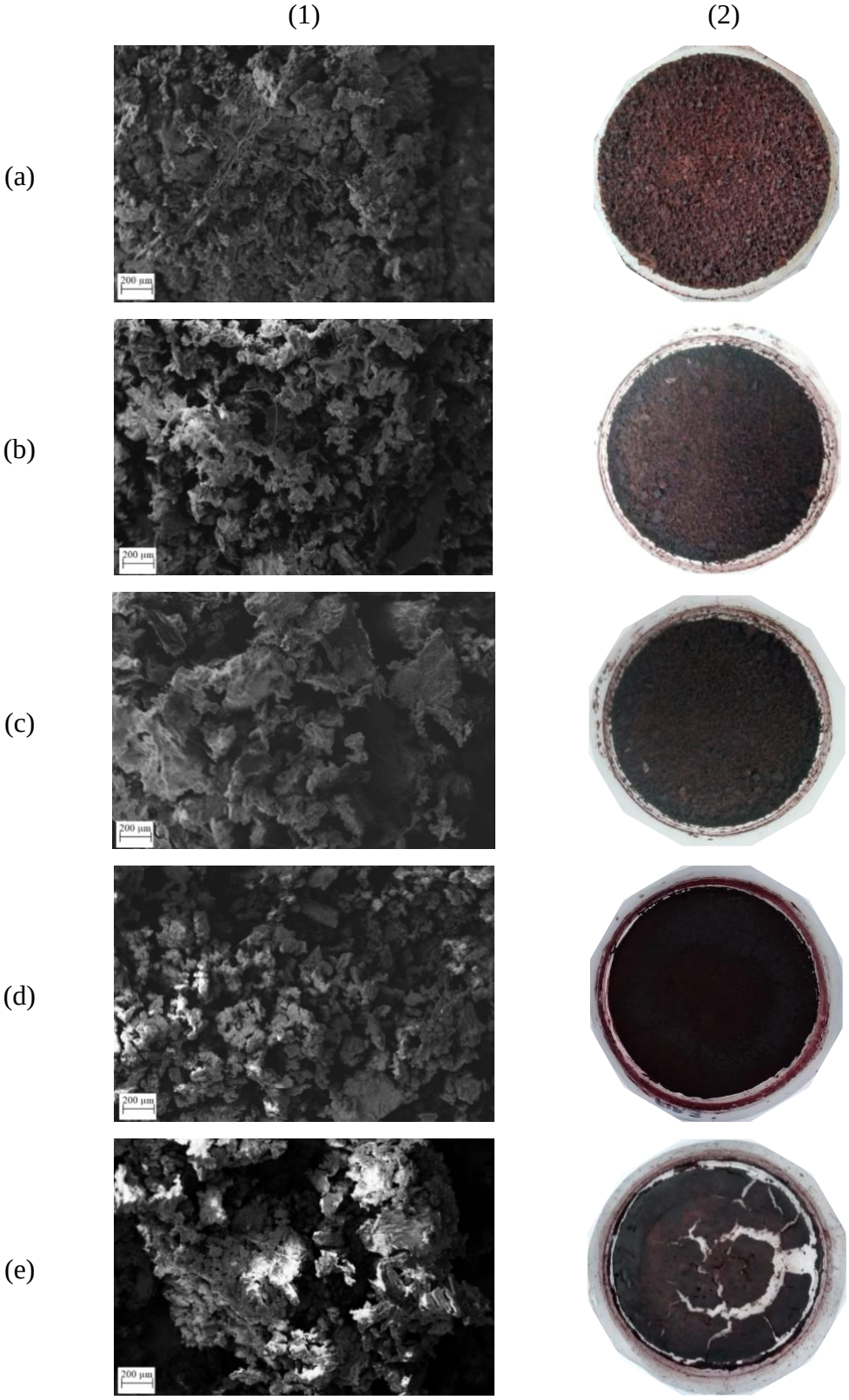

Figure 3 – (1) Scanning electron micrographs and (2) macrographs of freeze-dried açai puree subjected to different treatments: (a) freeze-drying; (b) freeze-drying + continuous near infrared radiation heating, NIRFD; (c) freeze-drying + near infrared radiation heating after 20% weight reduction, $NIRFD_{20\%WR}$; (d) freeze-drying + continuous far infrared radiation heating, FARFD; and (e) freeze-drying + far infrared radiation heating after 20% weight reduction, $FARFD_{20\%WR}$.

3.5.3 Water activity (a_w) and color

Water activity of samples was not statistically different between treatments (p>0.05), ranging from 0.38 to 0.40 (Table 3). In drying processes, a water activity value lower than 0.5 is critical to suppress microbial growth and to reduce reaction rates, including the inhibition of enzymatic and hydrolytic activities (Pittia & Antonello, 2015). Thus, the results reveal that IRFD can provide constant aw values for long-term storage.

Table 3 – Water activity (a_w) and color values (L*, a*, b*, $h°$) of freeze-dried açai puree subjected to freeze-drying (FD), near-infrared-assisted freeze-drying (NIRFD), freeze-drying + near-infrared heating after 20% weight reduction ($NIRFD_{20\%WR}$), far-infrared-assisted freeze-drying (FARFD) and, freeze-drying + far-infrared heating after 20% weight reduction ($FARFD_{20\%WR}$).

	a_w	L*	a*	b*	h^o
FD	0.38 ± 0.06	32.73 ± 0.33^{a}	5.73 ± 0.42	9.63 ± 0.15	59.23 ± 1.44^{a}
NIRFD	0.39 ± 0.00	31.88 ± 0.36^{b}	4.98 ± 0.26	9.43 ± 0.34	62.03 ± 0.99^{ab}
$NIRFD_{20\% WR}$	0.40 ± 0.16	31.78 ± 0.16^{bc}	5.25 ± 0.33	9.80 ±0.15	61.85 ± 1.24^{ab}
FARFD	0.38 ± 0.03	31.78 ± 0.40^{bc}	5.68 ± 0.35	9.48 ± 0.20	59.20 ± 2.06^{a}
$FARFD_{20\% WR}$	0.40 ± 0.03	31.22 ± 0.11^{c}	4.95 ± 0.40	9.63 ± 0.56	62.85 ± 0.75^{b}

Note: Values correspond to the mean and standard deviation. Means followed by the same letter do not differ according to Tukey's post-hoc test (p<0.05).

The color of the dehydrated açai puree was measured in the L*a*b* color space, Table 3. Resulting samples had a dark color, with L* ranging from 31.22 to 32.73. For this parameter, all IRFD treatments were significantly different to control (p<0.05; Table 3). IRFD contributed to a darker product (lower L* value) compared to FD, as seen in Figure 3. The loss of lightness in IRFD treatments can be attributed to Maillard browning reactions, since the association of the high fructose content in the acai puree with the higher temperature used in IRFD treatments (compared to FD) generated dark compounds (Wang et al., 2015).

There was no statistical difference (p>0.05) between treatments regarding a* and b*. Açai samples had a* values ranging from 4.95 to 5.73, showing a red hue. Açai puree is rich in anthocyanins, the pigment responsible for the orange, red, blue and violet colors in different fruits and flowers (Khoo, Azlan, Tang, & Lim, 2017). Values for b* ranged from 9.43 to 9.80 showing yellow color.

3.6 Bioactive Compounds of freeze-dried açai puree

The content of bioactive compounds of the powdered açai puree can be found in Table 4. Total phenolic content (TPC) was not affected by IR heating during the freeze-drying process, since there was no significant difference between treatments ($p>0.05$), ranging from 963.44 to 1025.60 mg GAE/100 g, Table 4. A higher TPC in freeze-dried açai puree was found by Oliveira et al. (2020) and Silveira et al. (2017), being 1405.03 and 1120 mg GAE/100 g, respectively.

Table 4 – Total phenolic content (mg GAE/100 g), antioxidant capacity (mg/100 g), and anthocyanin content (mg/100 g) of freeze-dried açai puree subjected to freeze-drying (FD), near-infrared-assisted freeze-drying (NIRFD), freeze-drying + near-infrared heating after 20% weight reduction (NIRFD20%WR), far-infrared-assisted freeze-drying (FARFD) and, freeze-drying + far-infrared heating after 20% weight reduction (FARFD20%WR).

	Total phenolic content (mg GAE/100 g)	Antioxidant capacity (%)	Anthocyanin content (mg cyanidin-3-glucoside/100 g)
FD	1025.60 ± 67.11[a]	59.91 ± 2.56 [a]	132.42 ± 15.07 [a]
NIRFD	968.40 ± 8.80 [a]	70.14 ± 1.48 [a]	151.07 ± 5.92 [a]
$NIRFD_{20\%WR}$	966.38 ± 17.41[a]	62.67 ± 1.97 [a]	148.53 ± 6.95 [a]
FARFD	963.44 ± 11.39 [a]	88.06 ± 8.44 [b]	93.88 ± 4.89 [b]
$FARFD_{20\%WR}$	988.4 ± 8.44 [a]	84.65 ± 0.98 [b]	90.37 ± 1.44 [b]

Note: Values correspond to the mean and standard deviation. Means followed by the same letter do not differ according to Tukey's post-hoc test ($p<0.05$).

A study by Wu et al. (2019) also found no difference in TPC between *Cordyceps militaris* samples dried by IRFD and FD at 40°C. However, when the drying temperature was higher than 40ºC, a reduction in TPC was reported, especially in IRFD. The same occurred in the work by Hnin, Zhang, Devahastin, and Wang (2019), where at temperatures higher than 45ºC, there was a reduction in TPC, with a more drastic decrease with IRFD. In the present study, the drying temperature in the IRFD was 35ºC, which might explain why no difference was found for TPC between FD and IRFD samples.

The antioxidant capacity of the powdered açai puree ranged from 59.91 to 88.06%, Table 4. There was significant increase ($p<0.05$) in treatments using the long wavelength lamp (FAR). A Maillard reaction generated antioxidant and darker products, as noted by the L* value in Table 3. According to Nooshkam, Varidi, and Bashash (2019), Maillard reaction products (MRPs) are widely produced in foods containing reducing sugars and amino acids during thermal processing and storage; these MRPs have excellent antioxidant capacity. NIRFD and $NIRFD_{20\%WR}$ samples had antioxidant capacity slightly higher than FD samples, however these did not result in significant differences between them ($p>0.05$).

Regarding anthocyanin, the compound responsible for most of the antioxidant capacity of açai, results ranged from 90.37 to 151.07 mg cyanidin-3-glucoside/100 g, Table 4, which is within the range reported by Heinrich et al. (2011) and Schauss et al. (2006). There was a significant reduction (p<0.05) in anthocyanin content in FAR samples (FARFD and $FARFD_{20\%WR}$) but not in NIR samples (NIRFD and $NIRFD_{20\%WR}$) when compared to control. Anthocyanins are very unstable to processing, as they are sensitive to factors such as temperature, light, pH, oxygen and others (Tonon, Brabet, & Hubinger, 2010). Drying using the FAR lamp may have rapidly increased the internal temperature through infrared radiation, resulting in anthocyanin degradation.

Açai has been widely consumed around the world due to its reputation as a fruit rich in several bioactive compounds, such as flavonoids, polyphenols and anthocyanins, which have been related to antioxidant, anti-inflammatory, anti-proliferative and cardioprotective properties. Thus, the drying process used to increase shelf life and facilitate logistics must also be adapted to maintain its nutritional characteristics. In this study, NIRFD and $NIR_{20\%WR}$ resulted in a product with characteristics more similar to the product dried by FD.

3.7 Functional properties

The results of the functional properties (bulk density; wettability; dispersibility; and water absorption capacity, WAC) of açai samples subjected to different freeze-drying treatments are shown in Table 5.

The bulk density of the dehydrated açai puree samples ranged from 0.178 to 0.297 kg/m^3. For dry products, low bulk density values are desired for packaging and transport considerations (Tonon, Freitas, & Hubinger, 2011). $FARFD_{20\%WR}$ samples had the highest density, 0.297 kg/m^3, whereas for the other treatments there was no statistical difference in this parameter. The density of the powder obtained with $FARFD_{20\%WR}$ was similar to the results of spray-dried açai juice powder from Tonon et al. (2011), where the bulk density ranged from 0.236 to 0.343 kg/m^3.

When the material is not thawed during the freeze-drying process, it results in a porous dry product (Berk, 2018; Pawar & Pratape, 2017). However, the $FARFD_{20\%WR}$ sample was collapsed after treatment and had a superficial crust, resulting in the highest density among treatments. According to Wang et al. (2015), the pore size distribution in the internal structure of dry products greatly affects bulk density and rehydration.

Table 5 – Bulk density (kg/m3), wettability (s), dispersibility (%) and water absorption capacity (WAC; %) of freeze-dried açai puree subjected to freeze-drying (FD), near-infrared-assisted freeze-drying (NIRFD), freeze-drying + near-infrared heating after 20% weight reduction (NIRFD20%WR), far-infrared-assisted freeze-drying (FARFD) and, freeze-drying + far-infrared heating after 20% weight reduction (FARFD20%WR).

	Bulk density (kg/m^3)	Wettability (s)	Dispersibility (%)	WAC (%)
FD	0.193 ± 0.010^{a}	16.5 ± 0.6^{a}	45.77 ± 4.35^{ab}	2.89 ± 0.11^{ab}
NIRFD	0.178 ± 0.010^{a}	24.5 ± 1.0^{b}	52.07 ± 1.67^{a}	3.29 ± 0.81^{a}
$NIRFD_{20\%WR}$	0.203 ± 0.019^{a}	14.0 ± 1.4^{a}	38.44 ± 1.48^{b}	2.44 ± 0.41^{ab}
FARFD	0.180 ± 0.008^{a}	19.5 ± 1.3^{c}	29.14 ± 3.72^{c}	2.74 ± 0.25^{ab}
$FARFD_{20\%WR}$	0.297 ± 0.010^{b}	29.5 ± 2.6^{d}	27.43 ± 3.71^{c}	2.01 ± 0.03^{b}

Note: Values correspond to the mean and standard deviation. Means followed by the same letter do not differ according to Tukey's post-hoc test ($p<0.05$).

The collapse generated during $FARFD_{20\%WR}$ also affected the wettability, dispersibility and WAC, resulting in the longest time to "absorb" liquid by capillary rise (29.5 s) and the lowest values for dispersibility and WAC (29.14% and 2.01%, respectively) when compared to the other treatments, Table 5. Probably, the dense layer in açai powders from this treatment caused the high interfacial tension between the powder surface and the liquid, partially preventing water entry.

Despite the collapse in $FARFD_{20\%WR}$, all powders from the various treatments had a fast wettability time, ranging from 14 to 29.5 s, which is extremely desirable. Among treatments, $NIRFD_{20\%\ WR}$ and FD samples had the shortest times to be completely wetted by a liquid. For other powdered foods, the wettability of dried soy milk, dates and yogurt was in the range of 57–308 s (Jinapong, Suphantharika, & Jamnong, 2008), 13–2258 s (Seerangurayar, Manickavasagan, Al-Ismaili, & Al-Mulla, 2018) and 374 s (Koç, Sakin-YIlmazer, Kaymak-Ertekin, & BalkIr, 2014), respectively.

Dispersibility is the ability of a powder to be wetted without the formation of dry lumps in the water. This measure indicates whether a food powder can be classified as "instant", showing good dispersibility when this value is above 67%, such as the case for tomato powder and instant coffee (> 99%) (Jaya & Das, 2004; Seerangurayar et al., 2018). In the present study, the dispersibility of açai powders ranged from 27.43 to 52.07% (Table 5), with a statistical difference between treatments ($p<0.05$). Treatments using long infrared radiation (FAR) reduced the dispersibility of powders. Drying using FAR heaters has a faster temperature increase in the surface of the sample compared to NIR (Sakai & Hanzawa, 1994), causing

structural damage and greater rigidity. The water absorption capacity had the same trend than dispersibility, with lower values ranging from 2.01 to 3.29%; there was a statistical difference between treatments (p<0.05).

4. Conclusion

Drying of açai puree by IRFD at long and short wavelengths significantly reduced the total drying time compared to traditional freeze-drying, specially NIRFD and FARFD, with 49.42 and 33.40% savings in drying time, respectively. Drying kinetics was estimated using Logarithmic, Diffusion approximation and Newton models. All models could precisely predict the drying process of IRFD.

IRFD caused changes in microstructure of açai puree powder. Using continuous IR (NIRFD and FARFD), the microstructure samples presented less compact structures with larger pores. For treatments $NIRFD_{20\%WR}$ and $FARFD_{20\%WR}$ açai puree samples showed collapsed structures. Besides that, drying by IRFD samples had darked color than FD samples due to Maillard reaction, which contributed to the increase their antioxidant activity. For a* and b* parameters there was no statistical difference between treatments.

Finally, this study demonstrated that NIRFD was the method that most preserved the antioxidant capacity, total phenolics and anthocyanin content of açai. NIRFD samples also had good values for density and wettability. Thus, IRFD using short-wave radiation (NIR) may be used instead of conventional FD, for it reduced total drying time without compromising the quality of the freeze-dried açai puree.

Acknowledgments

The authors thank FAPEMIG (Research Support Foundation of the State of Minas Gerais), CNPq (National Council for Scientific and Technological Development), and CAPES (Coordination of Improvement of Higher Level Personnel) for financial support and scholarships. The authors would also like to thank the Laboratory of Electron Microscopy and Analysis of Ultrastructural Federal University of Lavras for supplying the equipment and technical support for experiments involving electron microscopy.

References

Antal, T., & Kerekes, B. (2016). Investigation of Hot Air- and Infrared-Assisted Freeze-Drying of Apple. *Journal of Food Processing and Preservation*, *40*(2), 257–269. https://doi.org/10.1111/jfpp.12603

Antal, T., Tarek-Tilistyák, J., Cziáky, Z., & Sinka, L. (2017). Comparison of Drying and Quality Characteristics of Pear (Pyrus Communis L.) Using Mid-Infrared-Freeze Drying and Single Stage of Freeze Drying. *International Journal of Food Engineering*, *13*(4), 21. https://doi.org/10.1515/ijfe-2016-0294

AOAC; Association of Official Analytical Chemists. (2006). *Official methods of analysis of AOAC International* (W. H. Latimer & G. W. Latimer (eds.); 18 ed.). AOAC International.

Arend, G. D., Adorno, W. T., Rezzadori, K., Di Luccio, M., Chaves, V. C., Reginatto, F. H., & Petrus, J. C. C. (2017). Concentration of phenolic compounds from strawberry (Fragaria X ananassa Duch) juice by nanofiltration membrane. *Journal of Food Engineering*, *201*, 36–41. https://doi.org/https://doi.org/10.1016/j.jfoodeng.2017.01.014

Berk, Z. (2009). Freeze drying (lyophilization) and freeze concentration. In Z. Berk (Ed.), *Food Process Engineering and Technology* (pp. 511–523). Academic Press. https://doi.org/10.1016/b978-0-12-812018-7.00023-3

Berk, Z. (2018). Freeze drying (lyophilization) and freeze concentration. *Food Process Engineering and Technology*, 567–581. https://doi.org/10.1016/b978-0-12-812018-7.00023-3

Bi, J., Chen, Q., Zhou, Y., Liu, X., Wu, X., & Chen, R. (2014). Optimization of Short- and Medium-Wave Infrared Drying and Quality Evaluation of Jujube Powder. *Food and Bioprocess Technology*, *7*(8), 2375–2387. https://doi.org/10.1007/s11947-013-1245-y

Brand-Williams, W., Cuvelier, M. E., & Berset, C. (1995). Use of a free radical method to evaluate antioxidant activity. *LWT - Food Science and Technology*, *28*(1), 25–30. https://doi.org/https://doi.org/10.1016/S0023-6438(95)80008-5

Brasil. (2006). Instrução Normativa nº68, de 12 de dezembro de 2006: Métodos Analíticos Oficiais Físico-Químicos, para Controle de Leite e Produtos Lácteos. *Ministério Da Agricultura, Pecuária e Abastecimento*, 141. https://wp.ufpel.edu.br/inspleite/files/2016/03/Instrução-normativa-n°-68-de-12-dezembro-de-2006.pdf

Cohen, K. O., Chisté, R. C., Mattietto, R. A., Paes, N. S., Oliveira, M. S. P., & Souza, H. A. L. (2007). *Caracterização físico-química da polpa de açaí oriunda da cultivar de açaizeiro BRS-Pará em diferentes meses de coleta*. Ciência e Tecnologia de Alimentos Em Benefício a Sociedade: Ligando a Agricultura à Saúde: Resumos.; SBCTA: Unicamp/FEA. https://ainfo.cnptia.embrapa.br/digital/bitstream/item/60267/1/1170.pdf

Costa, H. C. B., Silva, D. O., & Vieira, L. G. M. (2018). Physical properties of açai-berry pulp and kinetics study of its anthocyanin thermal degradation. *Journal of Food Engineering*, *239*, 104–113. https://doi.org/10.1016/j.jfoodeng.2018.07.007

Das, I., & Das, S. K. (2010). Emitters and Infrared Heating System Design. In Z. Pan & G. G. Atungulu (Eds.), *Infrared Heating for Food and Agricultural Processing* (1st ed., pp. 57–88). Taylor & Francis Group. https://doi.org/10.1201/9781420090994-c4

Doymaz, I. (2014). Suitability of Thin-Layer Drying Models for Infrared Drying of Peach Slices. *Journal of Food Processing and Preservation*, *38*(6), 2232–2239. https://doi.org/10.1111/jfpp.12277

Fellows, P. J. (2009). Freeze drying and freeze concentration. In *Food Processing Technology Principles and Practice* (3rd ed., pp. 687–699). Woodhead Publishing Series. https://doi.org/10.1533/9781845696344.4.687

Hashimoto, A., Oshita, S., Yamazaki, Y., & Shimizu, M. (1994). Drying characteristics of gelatinous materials irradiated by infrared radiation. In *Drying Technology* (Issue 5, pp. 1029–1052). https://doi.org/10.1080/07373939408960987

Heinrich, M., Dhanji, T., & Casselman, I. (2011). Açai (Euterpe oleracea Mart.) - A phytochemical and pharmacological assessment of the species' health claims. *Phytochemistry Letters*, *4*(1), 10–21. https://doi.org/10.1016/j.phytol.2010.11.005

Hnin, K. K., Zhang, M., Devahastin, S., & Wang, B. (2019). Influence of Novel Infrared Freeze Drying of Rose Flavored Yogurt Melts on Their Physicochemical Properties, Bioactive Compounds and Energy Consumption. *Food and Bioprocess Technology*, *12*(12), 2062–2073. https://doi.org/10.1007/s11947-019-02368-x

Hnin, K. K., Zhang, M., Li, Z., & Wang, B. (2019). Comparison of quality aspects and energy consumption of restructured taro and potato chips under three drying methods. *Journal of Food Process Engineering*, *42*(7), 1–13. https://doi.org/10.1111/jfpe.13249

Hua, T.-C., Liu, B.-L., & Zhang, H. (2010). Fundamentals of Freeze Drying. *Freeze-Drying of Pharmaceutical and Food Products*, 18–67. https://doi.org/10.1533/9781845697471.18

İlter, I., Akyıl, S., Devseren, E., Okut, D., Koç, M., & Kaymak Ertekin, F. (2018). Microwave and hot air drying of garlic puree: drying kinetics and quality characteristics. *Heat and Mass Transfer/Waerme- Und Stoffuebertragung*, *54*(7), 2101–2112. https://doi.org/10.1007/s00231-018-2294-6

Jaya, S., & Das, H. (2004). Effect of maltodextrin, glycerol monostearate and tricalcium phosphate on vacuum dried mango powder properties. *Journal of Food Engineering*, *63*(2), 125–134. https://doi.org/10.1016/S0260-8774(03)00135-3

Jiang, H., Zhang, M., Mujumdar, A. S., & Lim, R. X. (2013). Analysis of Temperature Distribution and SEM Images of Microwave Freeze Drying Banana Chips. *Food and Bioprocess Technology*, *6*(5), 1144–1152. https://doi.org/10.1007/s11947-012-0801-1

Jinapong, N., Suphantharika, M., & Jamnong, P. (2008). Production of instant soymilk powders by ultrafiltration, spray drying and fluidized bed agglomeration. *Journal of Food Engineering*, *84*(2), 194–205. https://doi.org/10.1016/j.jfoodeng.2007.04.032

Khampakool, A., Soisungwan, S., & Park, S. H. (2019). Potential application of infrared assisted freeze drying (IRAFD) for banana snacks: Drying kinetics, energy consumption, and texture. *LWT - Food Science and Technology*, *99*(October 2018), 355–363. https://doi.org/10.1016/j.lwt.2018.09.081

Khampakool, A., Soisungwan, S., You, S. G., & Park, S. H. (2020). Infrared assisted freeze-drying (IRAFD) to produce shelf-stable insect food from protaetia brevitarsis (white-spotted flower chafer) Larva. *Food Science of Animal Resources*, *40*(5), 813–830. https://doi.org/10.5851/KOSFA.2020.E60

Khoo, H. E., Azlan, A., Tang, S. T., & Lim, S. M. (2017). Anthocyanidins and anthocyanins: Colored pigments as food, pharmaceutical ingredients, and the potential health benefits. *Food and Nutrition Research*, *61*(1), 0–21. https://doi.org/10.1080/16546628.2017.1361779

Koç, B., Sakin-YIlmazer, M., Kaymak-Ertekin, F., & BalkIr, P. (2014). Physical properties of yoghurt powder produced by spray drying. *Journal of Food Science and Technology*, *51*(7), 1377–1383. https://doi.org/10.1007/s13197-012-0653-8

Krishnamurthy, K., Khurana, H. K., Jun, S., Irudayaraj, J., & Demirci, A. (2008). Infrared Heating in Food Processing: An Overview. *COMPREHENSIVE REVIEWS IN FOOD SCIENCE AND FOOD SAFETY*, *7*, 13. https://doi.org/https://doi.org/10.1111/j.1541-4337.2007.00024.x

Lin, Y. P., Lee, T. Y., Tsen, J. H., & King, V. A. E. (2007). Dehydration of yam slices using FIR-assisted freeze drying. *Journal of Food Engineering*, *79*(4), 1295–1301. https://doi.org/10.1016/j.jfoodeng.2006.04.018

Lin, Y. P., Tsen, J. H., & King, V. A. E. (2005). Effects of far-infrared radiation on the freeze-drying of sweet potato. *Journal of Food Engineering*, *68*(2), 249–255. https://doi.org/10.1016/j.jfoodeng.2004.05.037

Liu, W., Zhang, M., Adhikari, B., & Chen, J. (2020). A novel strategy for improving drying efficiency and quality of cream mushroom soup based on microwave pre-gelatinization and infrared freeze-drying. *Innovative Food Science and Emerging Technologies*, *66*(September), 102516. https://doi.org/10.1016/j.ifset.2020.102516

Nooshkam, M., Varidi, M., & Bashash, M. (2019). The Maillard reaction products as food-born antioxidant and antibrowning agents in model and real food systems. *Food Chemistry*, *275*(September 2018), 644–660. https://doi.org/10.1016/j.foodchem.2018.09.083

Oliveira, A. R., Ribeiro, A. E. C., Oliveira, É. R., Garcia, M. C., Soares Júnior, M. S., & Caliari, M. (2020). Structural and physicochemical properties of freeze-dried açaí pulp (Euterpe oleracea mart.). *Food Science and Technology*, *40*(2), 282–289. https://doi.org/10.1590/fst.34818

Orrego, A. C. E. (2008). *Congelación y liofilización de alimentos* (UNIVERSIDAD NACIONAL DE COLOMBIA-GOBERNACIÓN DE CALDAS (ed.); 1st ed., Issue December). Artes Gráficas Tizan Ltda.

Pacheco-Palencia, L. A., Duncan, C. E., & Talcott, S. T. (2009). Phytochemical composition and thermal stability of two commercial açai species, Euterpe oleracea and Euterpe precatoria. *Food Chemistry*, *115*(4), 1199–1205. https://doi.org/10.1016/j.foodchem.2009.01.034

Pan, Z., & Atungulu, G. G. (2010). *Infrared Heating for food agricultural processing* (1st ed.). CRC Press.

Pan, Z., Shih, C., McHugh, T. H., & Hirschberg, E. (2008). Study of banana dehydration using sequential infrared radiation heating and freeze-drying. *LWT - Food Science and Technology*, *41*(10), 1944–1951. https://doi.org/10.1016/j.lwt.2008.01.019

Pavan, M. A., Schmidt, S. J., & Feng, H. (2012). Water sorption behavior and thermal analysis of freeze-dried, Refractance Window-dried and hot-air dried açaí (Euterpe oleracea Martius) juice. *LWT - Food Science and Technology*, *48*(1), 75–81. https://doi.org/10.1016/j.lwt.2012.02.024

Pawar, S. B., & Pratape, V. M. (2017). Fundamentals of Infrared Heating and Its Application in Drying of Food Materials: A Review. *Journal of Food Process Engineering*, *40*(1), 1–15. https://doi.org/10.1111/jfpe.12308

Pittia, P., & Antonello, P. (2015). Safety by Control of Water Activity: Drying, Smoking, and Salt or Sugar Addition. In V. Prakash, O. Martín-Belloso, L. Keener, S. Astley, S. Braun, H. McMahon, & H. Lelieveld (Eds.), *Regulating Safety of Traditional and Ethnic Foods* (Academic P, pp. 7–28). Elsevier Inc. https://doi.org/10.1016/B978-0-12-800605-4.00002-5

Rastogi, N. K. (2021). Infrared Heating in Drying Operations. In *Innovative Food Processing Technologies: A Comprehensive Review* (pp. 1–21). Elsevier. https://doi.org/10.1016/b978-0-08-100596-5.22671-1

Ratti, C. (2013). Freeze drying for food powder production. In *Handbook of Food Powders: Processes and Properties* (1st ed., pp. 57–84). Woodhead Publishing Limited. https://doi.org/10.1533/9780857098672.1.57

Riadh, M. H., Ahmad, S. A. B., Marhaban, M. H., & Soh, A. C. (2014). Infrared Heating in Food Drying: An Overview. *Drying Technology*, *3*, 322–335. https://doi.org/10.1080/07373937.2014.951124

Sakai, N., & Hanzawa, T. (1994). Applications and advances in far-infrared heating in Japan. *Trends in Food Science and Technology*, *5*(11), 357–362. https://doi.org/10.1016/0924-2244(94)90213-5

Salehi, F., & Kashaninejad, M. (2018). Modeling of moisture loss kinetics and color changes in the surface of lemon slice during the combined infrared-vacuum drying. *Information Processing in Agriculture*, *5*(4), 516–523. https://doi.org/10.1016/j.inpa.2018.05.006

Schauss, A. G., Wu, X., Prior, R. L., Ou, B., Patel, D., Huang, D., & Kababick, J. P. (2006). Phytochemical and Nutrient Composition of the Freeze-Dried Amazonian Palm Berry, Euterpe oleraceae Mart. (Acai). *Journal of Agricultural and Food Chemistry*, *54*, 8598–8603. https://doi.org/10.1021/jf060976g

Seerangurayar, T., Manickavasagan, A., Al-Ismaili, A. M., & Al-Mulla, Y. A. (2018). Effect of carrier agents on physicochemical properties of foam-mat freeze-dried date powder. *Drying Technology*, *36*(11), 1292–1303. https://doi.org/10.1080/07373937.2017.1400557

Shih, C., Pan, Z., McHugh, T., Wood, D., & Hirschberg, E. (2013). Sequential Infrared Radiation and Freeze-Drying Method for Producing Crispy Strawberries. *Transactions of the ASABE*, *51*(1), 205–216. https://doi.org/10.13031/2013.24205

Silva, H. R., Assis, D. da C. de, Prada, A. L., Silva, J. O. C., Sousa, M. B. de, Ferreira, A. M., Amado, J. R. R., Carvalho, H. de O., Santos, A. V. T. de L. T. dos, & Carvalho, J. C. T. (2019). Obtaining and characterization of anthocyanins from Euterpe oleracea (açaí) dry extract for nutraceutical and food preparations. *Revista Brasileira de Farmacognosia*, *29*(5), 677–685. https://doi.org/10.1016/j.bjp.2019.03.004

Silveira, T. F. F., de Souza, T. C. L., Carvalho, A. V., Ribeiro, A. B., Kuhnle, G. G. C., & Godoy, H. T. (2017). White açaí juice (Euterpe oleracea): Phenolic composition by LC-ESI-MS/MS, antioxidant capacity and inhibition effect on the formation of colorectal cancer related compounds. *Journal of Functional Foods*, *36*, 215–223. https://doi.org/10.1016/j.jff.2017.07.001

Singleton, V. L., & Rossi, J. A. (1965). Colorimetry of Total Phenolics with Phosphomolybdic-Phosphotungstic Acid Reagents. *American Journal of Enology and Viticulture*, *16*(3), 144 LP – 158. http://www.ajevonline.org/content/16/3/144.abstract

TechNavio. (2021). *Global Acai Berry Products Market 2021-2025*. TechNavio. https://www.researchandmarkets.com/reports/5062046/global-acai-berry-products-market-2021-2025#rela1-4390881

Tonon, R. V., Alexandre, D., Hubinger, M. D., & Cunha, R. L. (2009). Steady and dynamic shear rheological properties of açai pulp (Euterpe oleraceae Mart.). *Journal of Food Engineering*, *92*(4), 425–431. https://doi.org/10.1016/j.jfoodeng.2008.12.014

Tonon, R. V., Brabet, C., & Hubinger, M. D. (2010). Anthocyanin stability and antioxidant activity of spray-dried açai (Euterpe oleracea Mart.) juice produced with different carrier agents. *Food Research International*, *43*(3), 907–914. https://doi.org/10.1016/j.foodres.2009.12.013

Tonon, R. V., Freitas, S. S., & Hubinger, M. D. (2011). Spray drying of açai (Euterpe oleraceae Mart.) juice: Effect of inlet air temperature and type of carrier agent. *Journal of Food Processing and Preservation*, *35*(5), 691–700. https://doi.org/10.1111/j.1745-4549.2011.00518.x

Türkyılmaz, M., Tağı, Ş., Dereli, U., & Özkan, M. (2013). Effects of various pressing programs and yields on the antioxidant activity, antimicrobial activity, phenolic content and colour of pomegranate juices. *Food Chemistry*, *138*(2), 1810–1818. https://doi.org/https://doi.org/10.1016/j.foodchem.2012.11.100

Vasconcelos, M. da S., Mota, E. F., Gomes-Rochette, N. F., Nunes-Pinheiro, D. C. S., Nabavi, S. M., & de Melo, D. F. (2019). Açai or Brazilian Berry (Euterpe oleracea). In S. M. Nabavi & A. S. Silva (Eds.), *Nonvitamin and Nonmineral Nutritional Supplements* (Academic P, pp. 131–133). Elsevier Inc. https://doi.org/10.1016/B978-0-12-812491-8.00017-5

Waghmare, R. B., Perumal, A. B., Moses, J. A., & Anandharamakrishnan, C. (2021). Recent Developments in Freeze Drying of Foods. In *Innovative Food Processing Technologies* (Vol. 3, pp. 82–99). Elsevier. https://doi.org/10.1016/B978-0-12-815781-7.00017-2

Wang, H. C., Zhang, M., & Adhikari, B. (2015). Drying of shiitake mushroom by combining freeze-drying and mid-infrared radiation. *Food and Bioproducts Processing*, *94*(August), 507–517. https://doi.org/10.1016/j.fbp.2014.07.008

Wu, L., Orikasa, T., Ogawa, Y., & Tagawa, A. (2007). Vacuum drying characteristics of eggplants. *Journal of Food Engineering*, *83*(3), 422–429. https://doi.org/10.1016/j.jfoodeng.2007.03.03

Wu, X., Zhang, M., & Bhandari, B. (2019). A novel infrared freeze drying (IRFD) technology to lower the energy consumption and keep the quality of Cordyceps militaris. *Innovative Food Science and Emerging Technologies*, *54*(December 2018), 34–42. https://doi.org/10.1016/j.ifset.2019.03.003

ARTIGO 2

Comparison of near and far infrared-assisted freeze-drying (IRFD) of blackberries (*Rubus* spp. variety Tupy)

Normas do periódico: Journal of Food Engineering
ISSN: 0260-8774
(versão submetida)

Natália Leite Oliveira[a*], Ana Cláudia Silveira Alexandre[a], Sérgio Henrique Silva[a], Jayne de Abreu Figueiredo[a], Adrise Aparecida Rodrigues[a], Jaime Vilela de Resende[a]

[a] Universidade Federal de Lavras, Box 3037, 37200-000, Lavras, Minas Gerais, Brazil

*Corresponding author: Oliveira, N. L. Department of Food Science, Federal University of Lavras. E-mail address: natalia.oliveira1@estudante.ufla.br

Abstract

This study evaluated the drying and final quality parameters of blackberries (*Rubus* spp.) using near- (NIR) and long-wave (FAR) infrared radiation-assisted freeze-drying (IRFD). Treatments included 1) conventional freeze-drying (FD); 2) near IRFD (NIRFD); 3) far IRFD (FARFD); and 4) and 5) IRFD after 40% weight reduction. IRFD reduced the drying time compared to FD (time saving up to 42.51%), with NIRFD being the fastest treatment due to the greater penetration depth. Blackberries had good final appearance and characteristic red color (h° = 32.9). Samples obtained using long-wave had higher hardness (10.13 N) compared to FD (6.98 N). This result influenced negatively rehydration ratio. Also, these treatments reduced the anthocyanins content. For total phenolic content, treatments using near-wave samples had significantly higher values (765.46 and 777.60 mg gallic acid/100 g). Thus, we demonstrated that NIRFD has potential for the production of dried blackberries, resulting in a product with good appearance, high nutritional content, faster rehydration capacity in a shorter time.

Keywords: Texture profile analysis; Drying kinetics; Phenolics, Anthocyanins; Collapse

1 Introduction

Blackberry (*Rubus* spp.) is a fruit of black color when ripe and sour to sweet-and-sour flavor. It grows in erect bushes and is actually an aggregate of drupelets that weighs about four to seven grams (Franceschinis et al., 2014). Consumers are attracted to its high nutritional value and physical and mental health benefits, which can be largely attributed to its content of vitamins and phenolic compounds, such as phenolic acids, tannins and anthocyanins (Franceschinis et al., 2014; Jacques & Zambiazi, 2011; Yamashita et al., 2017). Fresh blackberries are a seasonal product that are highly perishable and have a short shelf life (Braga et al., 2019; Madrid & Beaudry, 2020). One of the ways to get around this problem while adding value to the product and diversifying its use is dehydration.

Freeze-drying is a dehydration process that results in high-value products, preserving their color and nutritional properties. However, it is an expensive drying method (Berk, 2009; Fellows, 2009; Orrego, 2008; Ratti, 2013). Infrared-assisted freeze-drying (IRFD) is a relatively new drying technique, first studied by Lin et al. (2005) in the dehydration of sweet potato slices. This process combines the advantages of infrared heating and lyophilization. By using infrared radiation (IR), it is possible to keep the characteristics of the product and, at the same time, increase the drying rate, thus reducing operating time and saving energy (Waghmare et al., 2021; Wu et al., 2019).

In the IRFD process, the product goes through the same steps as the conventional freeze-drying. The product is first frozen and then subjected to low pressures, losing moisture by sublimation and desorption during the primary and secondary drying, respectively (Berk, 2009; Fellows, 2009; Orrego, 2008). However, in IRFD, the energy required for sublimation is provided by infrared radiation (IR) instead of heating plates, which increases heat transfer rates (Pan & Atungulu, 2010).

IR is the portion of the electromagnetic spectrum that covers wavelengths from 0.75 to 1,000 μm (Pan & Atungulu, 2010; Sandu, 1986). IR is usually subdivided into three regions: near IR (NIR; 0.78–1.4 μm), middle IR (MIR; 1.4–3.0 μm) and far IR (FAR; 3.0-1000 μm). When the wavelength of the radiation source matches the spectral absorption of the irradiated product, the substance absorbs a large amount of infrared energy. This alters the movement of its molecules, causing the transformation of infrared radiation into rotational energy, which in turn causes an increase in temperature and the evaporation of water (Pan & Atungulu, 2010;

Pawar & Pratape, 2017). As a result, the drying process is significantly accelerated (Antal et al., 2017).

Several works have proven that IRFD reduced drying time without compromising the quality of various products when compared to conventional freeze-drying, including mushroom (*Cordyceps militaris*) (Wu et al., 2019) and apple pieces (Antal & Kerekes, 2016) by IRFD at the FAR wavelength. In addition, nutrient retention, rehydration rate and firmness were similar to freeze-dried products. Continuous NIR-assisted FD reduced drying time in banana snacks and even improved crispness (Khampakool et al., 2019). It also contributed to a faster drying time for powdered mushroom cream soup (Liu et al., 2020), rose-flavored yogurt (Hnin et al., 2019), and potato and taro chips (Hnin et al., 2019) without compromising physicochemical and textural properties. In a recent study, Oliveira et al. (2021) reported that the use of short-wavelength IR coupled to freeze-drying was ideal for açai puree drying, saving 49% of time when compared to conventional freeze-drying while maintaining the bioactive compounds of this product.

As exposed, IRFD contributes to the reduction of drying time, resulting in products with high added value. However, no research has compared different IR regions applied at different stages of the freeze-drying process of whole fruits. Thus, the object of this work was to evaluate and compare different freeze-drying settings, including treatments with auxiliary short- (NIR) and long-wave (FAR) infrared radiation applied during the entire drying process or beginning at the secondary drying, observing the economic, physicochemical and nutritional aspects.

2 Materials and Methods

2.1 Materials

Frozen blackberries (*Rubus* spp. variety Tupy) were purchased at stores in Lavras, Minas Gerais, Brazil, and stored at -75 ºC until the beginning of the drying process to minimize quality losses. Near (NIR) (TheraBulb, E27, China) and long (FAR) (Heating, ND-22, China) lamps were also obtained.

2.2 Infrared freeze-drying system (IRFD)

A freeze-dryer (L4KR, Edwards, São Paulo, Brazil) was customized by coupling it to an infrared heating system (Supplementary material). The equipment consisted of an acrylic

chamber, condenser and cooling coil at -40 ºC, a vacuum pump at 99.8 Pa, energy supply system and infrared lamps, temperature controller (thermostat), and weight and temperature (type T thermocouples) sensors.

Two types of IR lamps were used: near infrared (NIR) (E27, TheraBulb, China) and long (FAR) (ND-22, Heating, China). They were fixed on the top of the acrylic chamber, 20 cm above samples. The internal temperature of the chamber was set between 30 and 33 ºC and controlled by a thermostat (XH-W3001, Vipxyc, China) and product temperature was measured by inserting Type T thermocouples (Copper-Constantan), 1.5 mm in diameter and 100 mm in length, at the geometric center of the blackberries. To monitor weight reduction, samples were placed on a scale also coupled to the data acquisition system.

2.3 Freezing and drying

For each treatment, samples of 50 g of frozen blackberries were placed in 12.7 cm Petri dishes and stored at -75 ºC (CL120-86 V, Coldlab, Piracicaba, Brazil) for 24 h prior to the freeze-drying process. After freeze-drying, samples were stored in desiccators containing silica gel until analysis.

2.4 Experimental design

Infrared-assisted freeze-drying trials were set up in a completely randomized design (CRD) with five treatments and four repetitions: 1) freeze-drying control treatment, FD; 2) freeze-drying + continuous near infrared radiation heating, NIRFD; 3) freeze-drying + near infrared radiation heating after 40% weight reduction, $NIRFD_{40\%WR}$; 4) freeze-drying + continuous far infrared radiation heating, FARFD; 5) freeze-drying + far infrared radiation heating after 40% weight reduction, $FARFD_{40\%WR}$

In the NIRFD and $NIRFD_{40\%WR}$ treatments, the NIR lamp was attached to the drying chamber of the freeze-dryer. While in FARFD and $FARFD_{40\%WR}$ the FAR lamp was used. For the continuous IRFD, NIRFD and FARFD treatments, IR heating occurred throughout the drying process. In the case of freeze drying after 40% mass loss, the IR lamp was turned off at the initial stage of freeze drying and then manually turned on when the sample weight was reduced by 40% ($NIRFD_{40\%WR}$ or $FARFD_{40\%WR}$).

2.5 Drying process

2.5.1 Monitoring of mass and temperature

Temperature was measured during the freeze-drying process by inserting Type T thermocouples (Copper-Constantan), 1.5 mm in diameter and 100 mm in length, at the geometric center of the blackberries. The thermocouples were connected to a signal conditioning system (SCXI-1000, National Instruments Corporation, Budapest, Hungary) using LabView 8.5 software (National Instruments Corporation, Newbury, Ireland). Data were recorded at 5 min intervals.

Weight reduction over time was determined by weighing samples every 2.5 min using a scale coupled to a data acquisition system. Trials were carried out until the moisture content in samples reached <8.0% dry basis.

2.5.2 Radiant energy

The amount of radiant energy required for each treatment was calculated according to Khampakool et al. (2019). First, total energy (E_T) required to sublime the ice from initial moisture content (M_0) to final moisture content (M_f) (Equation 1):

$$E_T = m \times (M_0 - M_f) \times L_S \quad (1)$$

where E_T is total energy (kJ), m is the sample mass (kg) and L_s is the latent heat for ice sublimation ($L_s = 2.834 \times 10^3$ kJ·kg^{-1}).

Radiant energy (E_{RD}) can be derived by subtracting the vacuum energy (E_{VC}) from the total energy (E_T), as shown on equation 2.

$$E_{RD} = E_T - E_{VC} \quad (2)$$

Where E_{RD} is radiant energy (kJ), E_T is total energy (kJ), and E_{VC} is vacuum energy (kJ).

For the freeze-drying control treatment, E_T was considered equal to E_{VC}. For IRFD treatments, vacuum energy ($E_{VC,IRFD}$) was calculated as the ratio of IRFD drying time (t_{IRFD}) to FD drying time (t_{FD}), as shown in Eq. 3:

$$E_{VC,IRFD} = E_T \times \frac{t_{IRFD}}{t_{FD}} \quad (3)$$

where $E_{VC,IRFD}$ is IRFD vacuum energy (kJ), t_{IRFD} is IRFD drying time (min), and t_{FD} is FD time (min).

2.5.3 Drying kinetics

There are several empirical drying kinetics models. The logarithmic (Equation 4), Page (Equation 5) and Newton (Equation 6) models were selected to describe the drying curve of the samples as a function of moisture ratio (MR) over time. These models have been widely used to characterize the drying kinetics of foods (Chakraborty et al., 2011; Giri & Prasad, 2007; Huang et al., 2021; Khampakool et al., 2019; Lin et al., 2005; Liu et al., 2020; Mujumdar et al., 2015; Wang et al., 2015).

$$MR = a \cdot exp\ exp\ (-K \cdot t)\ + c \quad (4)$$

$$MR = exp(-kt^n) \quad (5)$$

$$MR = exp\ (-K \cdot t) \quad (6)$$

Where *MR* is the moisture ratio, *K* is the drying constant (h^{-1}), *t* is the time (h), *N* is the shape factor; and *a*, *b*, *c* are constants determined by the experimental data.

The dimensionless moisture ratio (MR) was calculated by Equation 7:

$$MR = \frac{u}{u_o} \quad (7)$$

where *u* is the water content during the drying process ($g_{water}/g_{dry\ matter}$) and u_o is the initial water content ($g_{water}/g_{dry\ matter}$).

The coefficient of determination (R^2) and the root mean square error (RMSE) were calculated to evaluate the goodness-of-fit of the models. The highest values of R^2 and the lowest values of RMSE were chosen for the fit.

2.6 Shrinkage

Shrinkage measurements were obtained by calculating the volume of four fruits for each treatment before and after the freeze-drying process. To calculate the volume, blackberries were considered to be ideal ellipsoids (Equation 8).

$$Volume = \frac{4\pi abc}{3} \quad (8)$$

Where *a*, *b* and *c* are the semi axes of the blackberries measured using a digital caliper (Model 100.170, Digimess, SP, Brazil).

According to Khalloufi and Ratti (2003), shrinkage occurs when there is a volume reduction greater than 15%. Thus, the reduction in volume ($\%Shrinkage$) was calculated by Equation 9:

$$\%Shrinkage = \frac{(V_i - V_f)}{V_i} \times 100 \quad (9)$$

where V_f and V_i are the final and initial volumes, respectively.

2.7 Water activity (a_w)

The water activity (a_w) of the freeze-dried blackberries was obtained using a dew point hygrometer (3TE, Aqualab - Decagon, Washington, USA) at 25 ºC ± 1 ºC.

2.8 Color

The color of the freeze-dried blackberry samples was measured with a colorimeter (CR-5, Konica Minolta Sensing Inc., Sakai, Japan) using a cylindrical coordinate system that includes L*, a*, b*, and hue angle (h◦). In this system, L* indicates lightness and ranges from 0 (black) to 100 (white), a* ranges from green to red (− a*, green; +a*, red), and b* ranges from blue to yellow (− b*, blue; +b*, yellow). Hue angle (h◦) is defined as starting at the +a* axis

and is expressed in degrees: 0◦ would be +a* (red), 90◦ would be +b* (yellow), 180◦ would be -a* (green), and 270◦ would be -b* (blue).

2.9 Texture profile analysis

Texture properties were determined with a TATX2i texturometer (Stable Microsystems, Godalming, England) using a P.20 cylinder probe and samples placed inside an acrylic tube. Tests were conducted under the following settings: pre-test speed of 3.0 $mm \cdot s^{-1}$, test speed of 5.0 $mm \cdot s^{-1}$, post-test speed of 1.0 $mm \cdot s^{-1}$, initial sample distance of 5.0 mm, time of 5.0 s. Values for hardness and chewiness were obtained, in Newtons and Joules, respectively.

2.10 Bioactive Compounds

2.10.1 Anthocyanin content

Total anthocyanin content was determined by the pH differential method, following the methodology by AOAC (2006). Around 0.5 (± 0.01) g of each sample was diluted in two buffer solutions (pH 1 and 4.5) and absorbance was measured at 520 and 700 nm in an UV/Visible spectrophotometer (Cary 50, Varian, Palo Alto, CA), with four technical replicates. Results were expressed in mg cyanidin-3-glucoside/100 g of lyophilized powder sample.

2.10.2 Total phenolic content

Total phenolic compounds (TPC) in freeze-dried blackberries were determined by Folin-Ciocalteu, as described by Singleton & Rossi (1965). Absorbance of 0.5 ± 0.01 g of each sample was measured in an UV/Visible spectrophotometer (Cary 50, Varian, Palo Alto, CA). The extraction solvent was used for the blank. All results were expressed as mg of gallic acid equivalents (GAE) per gram of freeze-dried sample.

2.10.3 Antioxidant capacity

Antioxidant activity was determined by the DPPH free radical scavenging method, according to Brand-Williams et al. (1995). Absorbance of 0.5 ± 0.01 g of each sample was

measured in an UV/ Visible spectrophotometer (Cary 50, Varian, Palo Alto, CA). Results were expressed as percentage.

2.11 Rehydration kinetics

To determine rehydration kinetics, the freeze-dried and previously weighed blackberries were immersed in 200 mL of distilled water at 25°C for 60 min. At 2.5 min intervals, samples were removed from the water, pat-dried with paper towels and weighed on an analytical scale (MARCA e outras informações), and then immersed again.

Changes in sample mass during water uptake was expressed as rehydration ratio (RR), that is, the ratio of the mass of the samples during water uptake to the mass of the original dry samples. The mean value of four replicates was calculated and plotted as a function of time.

2.12 Statistical analysis

The results of each analysis were subjected to analysis of variance (ANOVA) with a significance level of 0.05. When ANOVA was significant, multiple comparisons between treatments were performed using Tukey's post hoc test (p = 0.05). Statistical tests were performed using Statistica® 10.0 Software (license number STA999K347150-W; StatSoft, Tulsa, USA).

3 Results and discussion

3.1 Drying process

3.1.1 Monitoring of mass and temperature

Figure 1a shows the temperature profile of blackberry samples under different freeze-drying treatments. First, the blackberries were frozen and then taken to the freeze dryer, where the first reading was ~-50°C, followed by a rapid rise in temperature. Three steps were observed: primary drying, in which the removal of free water occurs by sublimation; secondary drying, where the removal of water in the food matrix occurs by desorption; and the interval where both primary and secondary drying coexist (Fellows, 2017; Orrego, 2008).

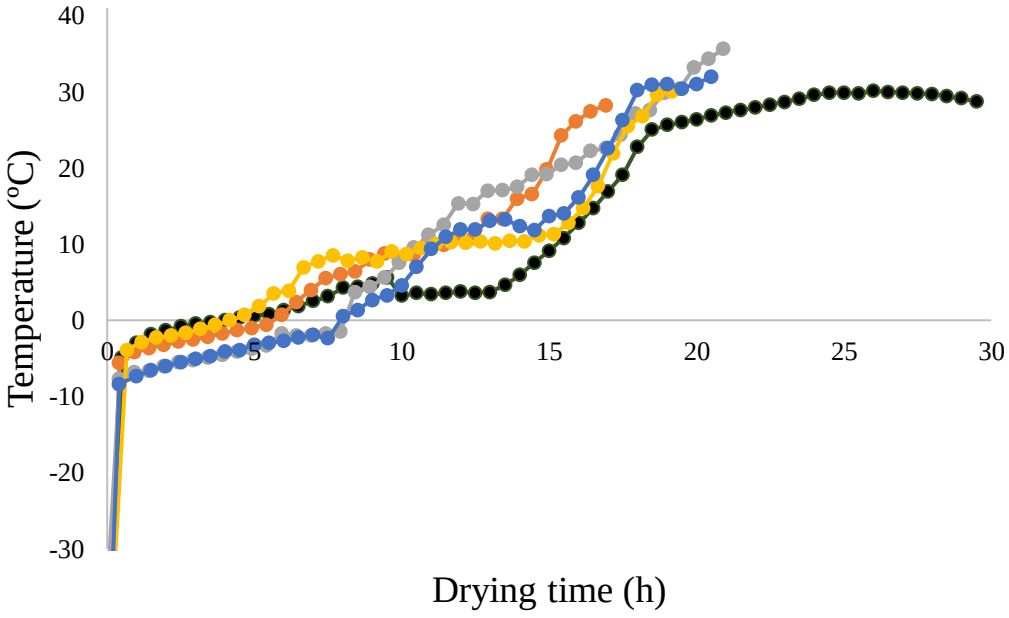

(a)

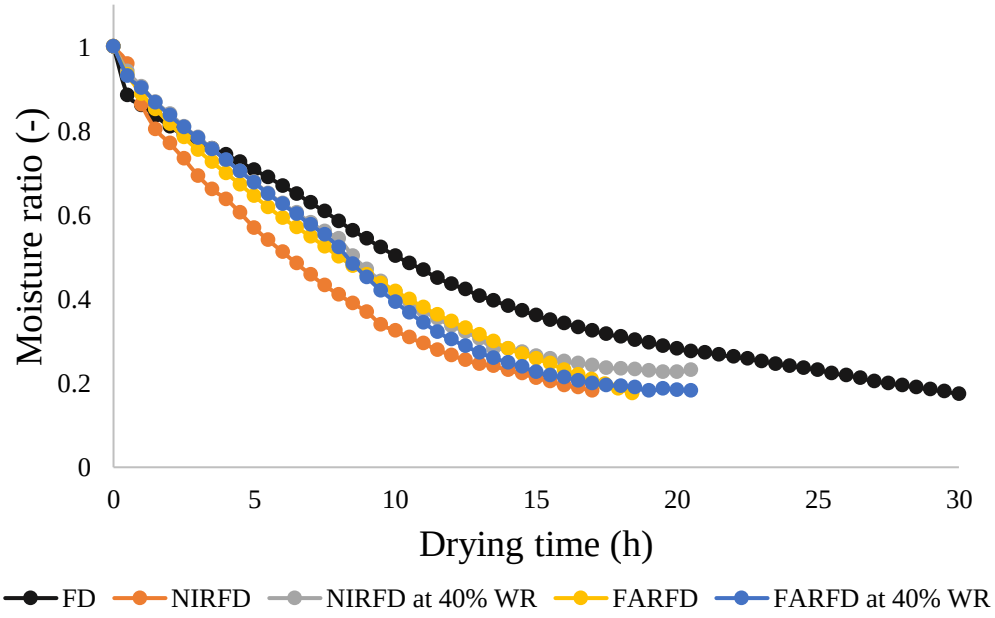

(b)

Figure 1 - (a) Temperature profiles and (b) Moisture ratio of blackberries (Rubus spp.) during freeze-dried (FD), near-infrared-assisted freeze-drying (NIRFD), freeze-drying + near-infrared heating after 40% weight reduction ($NIRFD_{40\%WR}$), far-infrared-assisted freeze-drying (FARFD) and, freeze-drying + far-infrared heating after 40% weight reduction ($FARFD_{40\%WR}$).

Primary drying took place between -10 and 5 ºC, depending on the treatment (Figure 1a). This stage has the longest duration and is characterized by the slight temperature variation over time; this is because all applied heat is used to sublimate ice from the sample to water vapor. The secondary drying started before the primary drying was completed, with both steps occurring simultaneously. As a consequence, the sublimation of the existing ice in the samples kept the food temperature under control. Temperatures during this intermediate step were between 5 and 14 ºC (Figure 1). The end of primary drying happened when the last bit of ice was sublimated. From this point onwards, the removal of water occurred only by desorption and there was a significant increase in temperature (Orrego, 2008), with sample temperature reaching ~30 ºC (Figure 1a).

As expected, FD samples remained longer in primary drying (~13.50 h), followed by $NIRFD_{40\%WR}$ and $FARFD_{40\%WR}$ samples (~8 h). Treatments where IR lighting was turned on after 40% weight reduction ($NIRFD_{40\%WR}$ and $FARFD_{40\%WR}$) contributed to speed the end of the primary drying; the UV radiation helps during the intermediate step, when the sublimation rate is greatly reduced in comparison to the beginning of the freeze-drying process. Treatments where freeze-drying occurred with continuous infrared radiation drastically reduced the time in primary drying; this step lasted 5 and 6 h for FARFD and NIRFD, respectively. IR during freeze-drying also accelerated the primary drying step in the work by Khampakool et al. (2020), Khampakool et al. (2019) and Hnin et al. (2019) on insect, banana and yogurt drying, respectively. The IR emitted by the lamps caused the energy to be absorbed by the components of the blackberry (water, sugar, etc), thus increasing molecular motion and consequently sample temperature (Antal et al., 2017; Pan & Atungulu, 2010; Pawar & Pratape, 2017). As a result, sublimation rate was increased and the time in primary drying reduced.

Figure 1b shows drying curves for the different treatments. Moisture ratio gradually decreased with increasing drying time and, as expected, the freeze-drying process was affected both by the use of infrared radiation and by the IR region used. FD took the longest time to complete the drying process (29.9 h) (Table 1). All IR-assisted treatments had significantly less drying time in relation to FD ($p < 0.05$), ranging from 17.2 to 21.3 h. NIRFD was the fastest treatment (17.2 h), reducing time by 42.51%, followed by FARFD (18.9 h and 36.5% time saving). These results demonstrate that drying blackberries under vacuum combined with infrared radiation increased the drying rate, thus revealing a potential for rapid drying at low temperatures (Khampakool et al. 2019; Salehi & Kashaninejad, 2018).

Table 1 - Total drying time, average drying rate, time saving, vacuum energy, and radiant energy of freeze-drying (FD), near-infrared-assisted freeze-drying (NIRFD), freeze-drying + near-infrared heating after 40% weight reduction ($NIRFD_{40\%WR}$), far-infrared-assisted freeze-drying (FARFD) and, freeze-drying + far-infrared heating after 40% weight reduction ($FARFD_{40\%WR}$) for drying blackberries (*Rubus* spp. variety Tupy).

Treatment	Total drying time (h)	Average drying rate (g/h)	Time saving[1] (%)	Vacuum energy (kJ)	Radiant energy (kJ)
FD	29.88 ± 0.24^{a}	1.67 ± 0.01^{a}	-	52.43 ± 0.43^{a}	-
NIRFD	17.18 ± 0.28^{b}	2.91 ± 0.04^{b}	42.51 ± 1.13^{a}	30.33 ± 0.49^{b}	22.10 ± 0.49^{a}
$NIRFD_{40\%WR}$	20.80 ± 0.27^{c}	2.40 ± 0.03^{c}	30.38 ± 1.42^{b}	36.72 ± 0.47^{c}	15.71 ± 0.47^{b}
FARFD	18.97 ± 0.29^{d}	2.63 ± 0.04^{d}	36.49 ± 1.45^{c}	33.50 ± 0.50^{d}	18.93 ± 0.50^{c}
$FARFD_{40\%WR}$	21.33 ± 1.04^{c}	2.34 ± 0.11^{c}	28.60 ± 3.98^{b}	37.66 ± 1.83^{c}	14.77 ± 1.83^{b}

[1] Percentage of time for the completion saved in comparison to control treatment (FD).
* Values correspond to the mean and standard deviation. Means followed by the same letter do not differ according to Tukey's post-hoc test ($p<0.05$).

The drying curves of $NIRFD_{40\%WR}$ and $FARFD_{40\%WR}$ had a sharp increase in their slope when the IR lamp was turned on after 40% weight reduction (Figure 1b), which happened ~8 h after the beginning of the drying process, thus increasing the drying rate. Both treatments also reduced the amount of time needed to completely dry the samples, saving ~29% when compared to FD. There was no statistical difference between the IR regions when lamps were turned on mid-process (after 40% weight reduction). In the treatments where IR was continuous (NIRFD and FARFD), NIR had better drying efficiency (2.91 g/h) than FAR (2.63 g/h), probably due to its greater penetration depth, since blackberries were about 24 mm thick. According to Bi et al. (2014), long-wave IR (4–100 μm) is absorbed on the surface of materials and is only suitable for thin layers, while medium- and short- wave IR (0.75–4 μm) are characterized by their higher radiation frequency and greater penetration depth, being more suitable for thicker agricultural samples, such as blackberries.

Another reason is that the -OH bonds in water molecules absorb more IR energy at wavelengths greater than 2.5 μm (Il'yasov & Krasnikov, 1991) while dry materials in most food products have a high transmissivity for wavelengths smaller than 2.5 μm (Sandu, 1986; Zhang et al., 2020). Therefore, as drying progressed, NIR was more efficient in heating the dry layer, and consequently reached a greater depth. However, the composition and structure of the product also determine the penetration depth of IR radiation (Rastogi, 2021).

3.1.2 Radiant energy

The energy consumption by sublimation represents almost half of the total energy consumption, among freezing, condensing water vapor and maintaining a vacuum. Therefore, by shortening the freeze-drying time, we can substantially decrease the energy consumption (Luo & Shu, 2017). Values for vacuum energy and radiant energy in FD and IRFD treatments can be seen in Table 1. FD required a vacuum energy of 52.43 kJ, whereas the different IRFD treatments required significantly less vacuum energy ($p < 0.05$), since the radiant energy provided the driving force for the sublimation of ice and subsequent rapid drying. Treatments using continuous IRFD had the lowest values for vacuum energy: 30.33 and 33.50 kJ for NIRFD and FARFD, respectively. As a consequence, IR contributed to save time during freeze-drying.

3.1.3 Drying kinetics

Table 2 shows the parameters for the logarithmic, Page and Newton models. All models had a good fit to the experimental data, with high values for the correlation coefficient ($0.98 \leq R^2 \leq 0.99$) and low values for RMSE ($0.002 \leq RMSE \leq 0.069$). Among the models tested, the logarithmic model was the one that best described the drying kinetics of the treatments ($R^2 \geq 0.994$). In the logarithmic model, the drying constant (K) increased from 0.059 to 0.125 h^{-1} with the addition of NIR to the freeze-drying system. K values in treatments where infrared radiation was used were higher than those in FD, given the process was faster as seen in the drying kinetics (Figure 1b). Treatments with continuous IR (NIRFD and FARFD) had the highest K values, followed by $NIRFD_{40\%WR}$ and $FARFD_{40\%WR}$. No trend was observed for the parameters A and C for the logarithm model.

Table 2 - Coefficients and goodness-of-fit of the Logarithmic, Page, and Newtonian models for drying blackberries (*Rubus* spp. variety Tupy) subjected to freeze-drying (FD), near-infrared-assisted freeze-drying (NIRFD), freeze-drying + near-infrared heating after 40% weight reduction ($NIRFD_{40\%WR}$), far-infrared-assisted freeze-drying (FARFD) and, freeze-drying + far-infrared heating after 40% weight reduction ($FARFD_{40\%WR}$).

Treatment	Logarithmic model $MR = a \cdot \exp(-K \cdot t) + c$					Page model $MR = exp(-K \cdot t^n)$				Newton model $MR = \exp(-K \cdot t)$		
	a	K (h^{-1})	c	R^2	RMSE	K (h^{-1})	N	R^2	RMSE	K (h^{-1})	R^2	RSME
FD	0.988	0.059	0.008	0.999	0.009	0.060	0.992	0.999	0.034	0.058	0.992	0.015
NIRFD	0.922	0.125	0.068	0.998	0.010	0.132	0.917	0.999	0.004	0.110	0.98	0.056
$NIRFD_{40\%WR}$	0.987	0.086	0.016	0.995	0.022	0.080	1.016	0.999	0.005	0.083	0.983	0.051
FARFD	0.881	0.118	0.051	0.998	0.013	0.160	0.846	0.998	0.016	0.114	0.992	0.034
$FARFD_{40\%WR}$	1.014	0.092	0.002	0.994	0.027	0.077	1.064	0.999	0.002	0.090	0.975	0.069

a,*N*, *c*: constants determined by the experimental data. *K*: drying constant (h^{-1}). R^2: coefficient of determination. RMSE: root mean square error

3.2 Physicochemical properties (shrinkage, a_w, color, texture)

Table 3 presents the results of shrinkage (%), water activity (a_w) and color parameters (L*, a*, b* and H°) of blackberry samples dried by FD and different treatments using IRFD. The reduction in the volume of blackberries was calculated based on the data of fresh and dried fruits. There was no significant difference ($p > 0.05$) between the different treatments, with a mean reduction of 36.50%. Shrinkage is a variable that shows structural changes and, ideally, it should be as low as possible. Despite the high value obtained, the dried blackberries had no change in shape and appearance, as can be seen in Figure 2.

Figure 2 - Blackberries dried prepared by: (a) freeze-dried (FD), (b) near-infrared-assisted freeze-drying (NIRFD), (c) freeze-drying + near-infrared heating after 40% weight reduction (NIRFD40%WR), (d) far-infrared-assisted freeze-drying (FARFD) and, (e) freeze-drying + far-infrared heating after 40% weight reduction (FARFD40%WR).

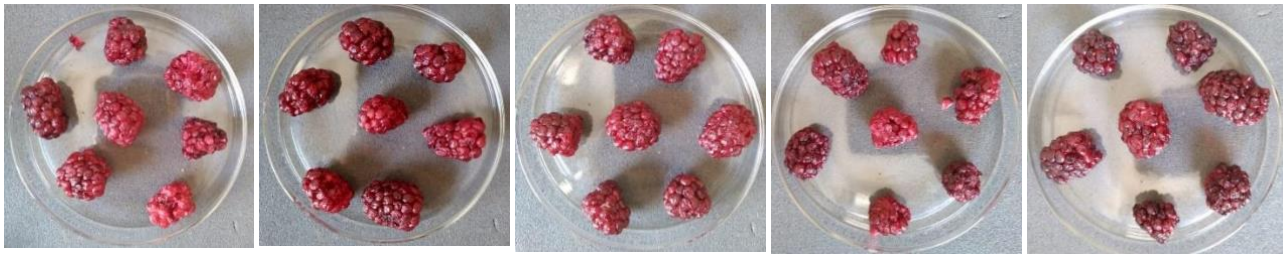

(a) (b) (c) (d) (e)

For a_w, no significant difference was observed between the IRFD and FD treatments ($p > 0.05$), with values ranging from 0.30 to 0.32. Values for a_w were satisfactory to guarantee the physical, chemical and microbiological stability of the dried blackberry samples. According to Damodaran (2019), values below 0.6 are ideal to avoid microbiological growth, and values between 0.20 and 0.40, for dehydrated foods, are considered stable regarding browning, lipid oxidation, microbial growth, hydrolytic and enzymatic reactions (Caliskan & Dirim, 2016).

In general, FD is superior to other drying methods regarding the preservation of the color, nutritional compounds and overall shape of food products (Khampakool et al., 2019). Infrared-assisted freeze-drying did not influence the appearance of dehydrated blackberries, since there was no statistical difference between treatments ($p > 0.05$) for any of the color parameters evaluated. L* values indicate how light or dark the analyzed products are (0 = black; 100 = white), with dried blackberries showing a darker hue (mean of 17.5). The value obtained was higher than the one reported by Franceschinis et al. (2014) for *in natura* blackberries, and lower than the one reported by the same author for dehydrated powdered blackberries. Freeze-dried blackberries had a mean value of 17.6 for a*, a parameter that ranges between green (-) and red (+). The results indicate that the dehydrated blackberries are red in color, just like the *in natura* fruits, as reported by Wu et al. (2021).

Table 3 - Shrinkage (%) and physicochemical parameters of drying blackberries subjected to freeze-drying (FD), near-infrared-assisted freeze-drying (NIRFD), freeze-drying + near-infrared heating after 40% weight reduction ($NIRFD_{40\%WR}$), far-infrared-assisted freeze-drying (FARFD) and, freeze-drying + far-infrared heating after 40% weight reduction ($FARFD_{40\%WR}$).

Treatment	Shrinkage (%)	a_w	L*	a*	b*	h^o
FD	39.00 ± 5.77	0.31 ± 0.01	18.3 ± 0.8	20.2 ± 2.1	11.4 ± 1.3	28.7 ± 2.9
NIRFD	30.55 ± 9.18	0.31 ± 0.00	19.2 ± 1.8	15.5 ± 0.9	10.6 ± 0.7	33.8 ± 2.1
$NIRFD_{40\%WR}$	32.48 ± 5.64	0.30 ± 0.02	17.3 ± 0.8	16.2 ± 2.4	10.8 ± 0.6	33.6 ± 2.0
FARFD	40.96 ± 2.95	0.32 ± 0.01	16.8 ± 1.4	19.6 ± 3.2	12.0 ± 0.6	32.0 ± 3.8
$FARFD_{40\%WR}$	35.55 ± 5.87	0.32 ± 0.02	17.0 ± 1.0	16.3 ± 2.3	11.5 ± 1.4	33.2 ± 2.8

Note: Values correspond to the mean and standard deviation. These values are not statistically significant ($p > 0.05$).

Color is a key quality attribute of a food product because the external appearance influences consumer choice and acceptability (Hnin, Zhang, Devahastin, et al., 2019). In this sense, the use of IR preserved the original appearance of the blackberries (Supplementary material). IRFD also did not change the color of dried bananas in the study by Khampakool et al. (2019) and shiitake mushroom samples in the research by Wang et al. (2015). On the other

hand, in the study by Hnin et al. (2019), all tested treatments changed the color of yogurt samples in relation to *in natura* yogurt but the total color difference of IRFD treatments were significantly smaller than FD.

The hardness and chewiness data of blackberry samples dried by FD and different IRFD treatments are shown in Table 4. Hardness is defined as the force (N) required to achieve a given deformation. Samples dried by IRFD required a greater force to deform (7.22 - 10.18 N) compared to FD samples (6.98 N). In addition, samples dried using long-wave IR (FAR) had higher hardness (10.08 and 10.18 for FARFD and $FARFD_{40\%WR}$, respectively). According to Singh et al. (2013), hardness is a parameter that is correlated to the moisture content of the product, however, in the present work, samples were dried until they reached roughly the same final moisture content (~8%). Khampakool et al. (2019) also reported that IRFD resulted in harder banana chips and attributed that this parameter was influenced by the drying rate and microstructure of the final product. For Hnin et al. (2019), the increase in hardness in IRFD is due to the denser parts of the product promoted by IR, resulting in high structural strength during texture measurement.

Table 4 - Texture profile analysis: hardness (N) and chewiness (J); and bioactive compounds: content of total phenolic compounds (TPC, $mg_{ácido\ gálico}/g_{amostra}$), antioxidant capacity (AC, %) and anthocyanin content (mg/100 g) of drying blackberries (*Rubus* spp. variety Tupy) subjected to freeze-drying (FD), near-infrared-assisted freeze-drying (NIRFD), freeze-drying + near-infrared heating after 40% weight reduction ($NIRFD_{40\%WR}$), far-infrared-assisted freeze-drying (FARFD) and, freeze-drying + far-infrared heating after 40% weight reduction ($FARFD_{40\%WR}$).

Treatment	Hardness (N)	Chewiness (J)	TPC (mg/100 g)	AC (%)	Anthocyanin (mg/ 100 g)
FD	6.98 ± 0.57^{a}	0.84 ± 0.12	732.64 ± 6.56^{a}	71.80 ± 2.52^{a}	178.00 ± 2.87^{a}
NIRFD	7.22 ± 0.73^{ab}	1.35 ± 0.39	765.46 ± 1.59^{b}	77.91 ± 0.33^{b}	176.94 ± 2.37^{a}
$NIRFD_{40\%WR}$	9.49 ± 0.65^{bc}	1.40 ± 0.38	777.60 ± 5.42^{b}	75.94 ± 2.26^{b}	177.93 ± 2.37^{a}
FARFD	10.08 ± 1.22^{c}	1.63 ± 0.53	665.33 ± 5.10^{c}	77.37 ± 0.43^{b}	150.73 ± 3.49^{b}
$FARFD_{40\%WR}$	10.18 ± 1.24^{c}	1.56 ± 0.46	702.12 ± 2.88^{d}	76.54 ± 1.56^{b}	163.80 ± 4.65^{c}

Note: Values correspond to the mean and standard deviation. Two consecutive letters of the same type indicate that the values are not statistically significant ($p < 0.05$) using the Tukey's test.

Chewiness is defined as the amount of work required to chew a sample to a state ready for swallowing (Meulleneti, 1998). This parameter ranged from 0.84 to 1.63, without differences between treatments ($p > 0.05$). This indicates that, even though IRFD fruits were

crunchier (as shown by their hardness value) due to the higher density on their surface caused by IR, the internal space of all treatments probably had multiple pores (a characteristic of freeze-dried products), which made all samples have the same chewiness regardless of treatment.

3.3 Bioactive compounds (anthocyanin content, total phenolic content and antioxidant capacity)

The most significant benefits of blackberries are due to their bioactive compounds and these were significantly affected ($p < 0.05$) by the drying method applied, as can be seen in Table 4. For total phenolic content (TPC), both the longer drying time and the IR wavelength used influenced this parameter. Treatments using short-wave infrared radiation had higher TPC values (765.46 and 777.60 mg gallic acid/100 g for NIRFD and NIRFD$_{40\%WR}$, respectively). On the other hand, treatments using the FAR lamp (especially FARFD) had the lowest TPC values. Other authors reported that there was a reduction in TPC using IRFD only when temperatures above 40 ºC were used, such as Wu et al. (2019) on FAR-assisted freeze-dried *Cordyceps militaris* samples, Hnin et al. (2021) on edible pink flowers, and Hnin et al. (2019a) on yogurt.

The hydroxyl radical scavenging activities of all samples were greater than 70%, indicating a strong antioxidant capacity (AC) for the blackberry samples. IRFD samples had a significantly higher AC than FD samples ($p < 0.05$). The samples obtained by NIRFD and FARFD had the highest AC (77.91 and 77.37%, respectively) although there was no statistical difference between themselves or between them and other IRFD samples (Table 4). It is possible the less time to IR exposure contributed to the preservation of this parameter.

Antal et al. (2017) reported that the use of IRFD caused the antioxidant capacity of pear samples to increase by up to 168% compared to the treatment without IR. The authors argued that far infrared has the ability to break the covalent bond and release antioxidants, therefore increasing the AC of the IR-assisted freeze-dried biomaterial. Oliveira et al. (2021) also found an increase in AC using IR lighting to assist the freeze-drying of açai samples. The authors concluded that the Maillard reaction that occurs during the heat processing of food products containing reducing sugars (fructose and glucose) and compounds containing amino acids (Nooshkam et al., 2019) may be responsible for this increase, since the products of this reaction have excellent antioxidant capacity.

The anthocyanin content in the dried blackberries ranged from 150.73 to 178.00 mg cyanidin-3-glucoside/100 g, as shown in Table 4. Anthocyanins are very unstable to processing, being sensitive to factors such as temperature, light, pH, oxygen and others (Tonon et al., 2010). Similar to the results for TPC, samples freeze-dried with long-wave IR had the lowest values for anthocyanin content (150.73 and 163.80 mg cyanidin-3-glucoside/100 g for FARFD and $FARFD_{40\%WR}$, respectively). There was no statistical difference for anthocyanin content values between NIRFD, $NIRFD_{40\%WR}$ and FD samples. FAR-assisted drying has a faster temperature increase on the surface of samples in comparison to NIR-assisted drying (Sakai & Hanzawa, 1994), which may explain the degradation of anthocyanins and total phenols.

3.4 Rehydration ratio

The rehydration behavior of dried products is a quality parameter that indicates the physical and chemical changes caused by the drying process (Lin et al., 2007). The rehydration ratio (RR) of freeze-dried blackberries over time is shown in Figure 3. Differences in RR values are related to the structural porosity and pore size on dried products (Bui et al., 2018). NIRFD samples had the highest values for RR throughout the entire time, while FARFD had the lowest values. May far-infrared heat the outer surface in the first place and then promote deformation and even waterproofing. FD, $NIRFD_{40\%WR}$ and $FARFD_{40\%WR}$ blackberries had only a slight difference in rehydration.

According to Lin et al. (2007) lower rehydration values are related to product shrinkage caused by strong heating and/or prolonged drying. Despite not having a significant difference, NIRFD showed the lowest shrinkage (30.55%) while FARFD had the highest (40.96%). Furthermore, FARFD samples had higher hardness, which was related to denser parts in the outer layer of these fruits; this hardened layer may have functioned as a barrier to water entry during rehydration. Antal et al. (2017) reported that there was low rehydration capacity in products where a collapsed surface layer was observed. The same authors also showed that the use of medium-wave IRFD increased the rehydration capacity when compared to conventional freeze-drying, and argued that the faster drying with IR may help samples to retain their porous and less dense structures, increasing its ability to absorb more water during the rehydration process. Liu et al. (2020) studied the rehydration of mushroom soup and observed that the IRFD treatment reduced the RR compared to FD, however the authors did not specify which IR wavelength was used.

Figure 3 - Effect of different drying methods on the rehydration characteristics of blackberries dried: freeze-dried (FD), near-infrared-assisted freeze-drying (NIRFD), freeze-drying + near-infrared heating after 40% weight reduction (NIRFD40%WR), far-infrared-assisted freeze-drying (FARFD) and, freeze-drying + far-infrared heating after 40% weight reduction (FARFD40%WR).

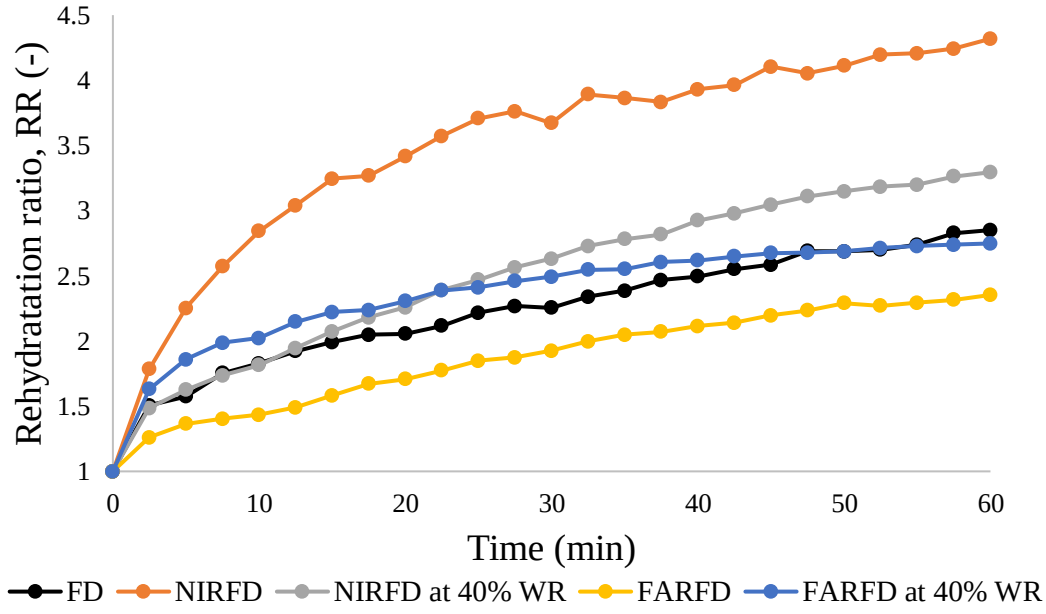

4 Conclusion

Here, we investigated the effect of short-wave and long-wave infrared-assisted freeze-drying on the drying efficiency and on the textural and nutritional properties of blackberries. IRFD increased the drying rate and reduced the primary drying, which led to time savings of 28.60 to 42.51% over FD. In addition, IRFD was able to preserve the original color and appearance of the blackberries.

NIRFD, which used continuous short-wave IR lighting, was more efficient than the other treatments, given that it reduced the time for complete dehydration while still preserving bioactive compounds such as total phenols and antioxidants. It also had high anthocyanin content and good rehydration capacity. On the other hand, FARFD (which used continuous long-wave IR lighting) compromised the total phenolics and anthocyanin content. It also resulted in harder dried fruits and lower rehydration ratio. There was no difference between IR wavelengths when lamps were turned on after 40% weight reduction (NIRFD$_{40\%WR}$ and

$FARFD_{40\%WR}$) with little variation between their parameters and a smaller variation in relation to the control treatment (FD).

Thus, IRFD, especially freeze-drying with continuous near infrared radiation heating, has good potential for the production of dried blackberries with high added value, as its final products have a good appearance and high nutritional content while saving time and energy.

Acknowledgments

The authors thank the financial support of FAPEMIG (Research Support Foundation of the State of Minas Gerais), CNPq (National Council for Scientific and Technological Development), and CAPES (Coordination of Improvement of Higher Level Personnel). The authors would also like to thank the Department of Food Science at Federal University of Lavras for supplying the equipment and technical support to perform the trials.

References

Antal, T., & Kerekes, B. (2016). Investigation of Hot Air- and Infrared-Assisted Freeze-Drying of Apple. *Journal of Food Processing and Preservation*, *40*(2), 257–269. https://doi.org/10.1111/jfpp.12603

Antal, T., Tarek-Tilistyák, J., Cziáky, Z., & Sinka, L. (2017). Comparison of Drying and Quality Characteristics of Pear (Pyrus Communis L.) Using Mid-Infrared-Freeze Drying and Single Stage of Freeze Drying. *International Journal of Food Engineering*, *13*(4), 21. https://doi.org/10.1515/ijfe-2016-0294

AOAC; Association of Official Analytical Chemists. (2006). *Official methods of analysis of AOAC International* (W. H. Latimer & G. W. Latimer (eds.); 18 ed.). AOAC International.

Berk, Z. (2009). Freeze drying (lyophilization) and freeze concentration. In Z. Berk (Ed.), *Food Process Engineering and Technology* (pp. 511–523). Academic Press. https://doi.org/10.1016/b978-0-12-812018-7.00023-3

Bi, J., Chen, Q., Zhou, Y., Liu, X., Wu, X., & Chen, R. (2014). Optimization of Short- and Medium-Wave Infrared Drying and Quality Evaluation of Jujube Powder. *Food and Bioprocess Technology*, *7*(8), 2375–2387. https://doi.org/10.1007/s11947-013-1245-y

Braga, M. B., Veggi, P. C., Codolo, M. C., Giaconia, M. A., Rodrigues, C. L., & Braga, A. R. C. (2019). Evaluation of freeze-dried milk-blackberry pulp mixture: Influence of adjuvants

over the physical properties of the powder, anthocyanin content and antioxidant activity. *Food Research International*, *125*(February), 108557. https://doi.org/10.1016/j.foodres.2019.108557

Brand-Williams, W., Cuvelier, M. E., & Berset, C. (1995). Use of a free radical method to evaluate antioxidant activity. *LWT - Food Science and Technology*, *28*(1), 25–30. https://doi.org/https://doi.org/10.1016/S0023-6438(95)80008-5

Bui, L. T. T., Coad, R. A., & Stanley, R. A. (2018). Properties of rehydrated freeze dried rice as a function of processing treatments. *LWT - Food Science and Technology*, *91*(December 2017), 143–150. https://doi.org/10.1016/j.lwt.2018.01.039

Caliskan, G., & Dirim, S. N. (2016). The effect of different drying processes and the amounts of maltodextrin addition on the powder properties of sumac extract powders. *Powder Technology*, *287*, 308–314. https://doi.org/10.1016/j.powtec.2015.10.019

Chakraborty, R., Bera, M., Mukhopadhyay, P., & Bhattacharya, P. (2011). Prediction of optimal conditions of infrared assisted freeze-drying of aloe vera (Aloe barbadensis) using response surface methodology. *Separation and Purification Technology*, *80*(2), 375–384. https://doi.org/10.1016/j.seppur.2011.05.023

Damodaran, S. (2019). Relações entre água e gelo nos alimentos. In *Química de Alimentos de Fennema* (5 ed., pp. 19–90). ArtMed.

Fellows, P. J. (2009). Freeze drying and freeze concentration. In *Food Processing Technology Principles and Practice* (3rd ed., pp. 687–699). Woodhead Publishing Series. https://doi.org/10.1533/9781845696344.4.687

Fellows, P. J. (2017). Freeze drying and freeze concentration. *Food Processing Technology*, 929–945. https://doi.org/10.1016/b978-0-08-100522-4.00023-7

Franceschinis, L., Salvatori, D. M., Sosa, N., & Schebor, C. (2014). Physical and Functional Properties of Blackberry Freeze- and Spray-Dried Powders. *Drying Technology*, *32*(2), 197–207. https://doi.org/10.1080/07373937.2013.814664

Giri, S. K., & Prasad, S. (2007). Drying kinetics and rehydration characteristics of microwave-vacuum and convective hot-air dried mushrooms. *Journal of Food Engineering*, *78*(2), 512–521. https://doi.org/10.1016/j.jfoodeng.2005.10.021

Hnin, K. K., Zhang, M., Devahastin, S., & Wang, B. (2019). Influence of Novel Infrared Freeze Drying of Rose Flavored Yogurt Melts on Their Physicochemical Properties, Bioactive Compounds and Energy Consumption. *Food and Bioprocess Technology*, *12*(12), 2062–2073. https://doi.org/10.1007/s11947-019-02368-x

Hnin, K. K., Zhang, M., Ju, R., & Wang, B. (2021). A novel infrared pulse-spouted freeze drying on the drying kinetics, energy consumption and quality of edible rose flowers. *Lwt*, *136*(P1), 110318. https://doi.org/10.1016/j.lwt.2020.110318

Hnin, K. K., Zhang, M., Li, Z., & Wang, B. (2019). Comparison of quality aspects and energy consumption of restructured taro and potato chips under three drying methods. *Journal of Food Process Engineering*, *42*(7), 1–13. https://doi.org/10.1111/jfpe.13249

Huang, D., Yang, P., Tang, X., Luo, L., & Sunden, B. (2021). Application of infrared radiation in the drying of food products. *Trends in Food Science and Technology*, *110*(October 2020), 765–777. https://doi.org/10.1016/j.tifs.2021.02.039

Il'yasov, S. G., & Krasnikov, V. V. (1991). *PHYSICAL PRINCIPLES OF INFRARED ERADIATION OF FOODSTUFFS* (A. P. Kotlobye (ed.)). Hemisphere Publishing Corporation.

Jacques, A. C. ., & Zambiazi, R. C. . (2011). Phytochemicals in blackberry [Fitoquímicos em amora-preta (Rubus spp)]. *Semina:Ciencias Agrarias*, *32*(1), 245–260. http://www.scopus.com/inward/record.url?eid=2-s2.0-79958737905&partnerID=40&md5=a976b6d03411fe1389d8f979a61a3249

Khalloufi, S., & Ratti, C. (2003). Quality deterioration of freeze-dried foods as explained by their glass transition temperature and internal structure. *Journal of Food Science*, *68*(3), 892–903. https://doi.org/10.1111/j.1365-2621.2003.tb08262.x

Khampakool, A., Soisungwan, S., & Park, S. H. (2019). Potential application of infrared assisted freeze drying (IRAFD) for banana snacks: Drying kinetics, energy consumption, and texture. *LWT - Food Science and Technology*, *99*(October 2018), 355–363. https://doi.org/10.1016/j.lwt.2018.09.081

Khampakool, A., Soisungwan, S., You, S. G., & Park, S. H. (2020). Infrared assisted freeze-drying (IRAFD) to produce shelf-stable insect food from protaetia brevitarsis (white-spotted flower chafer) Larva. *Food Science of Animal Resources*, *40*(5), 813–830. https://doi.org/10.5851/KOSFA.2020.E60

Lin, Y. P., Lee, T. Y., Tsen, J. H., & King, V. A. E. (2007). Dehydration of yam slices using FIR-assisted freeze drying. *Journal of Food Engineering*, *79*(4), 1295–1301. https://doi.org/10.1016/j.jfoodeng.2006.04.018

Lin, Y. P., Tsen, J. H., & King, V. A. E. (2005). Effects of far-infrared radiation on the freeze-drying of sweet potato. *Journal of Food Engineering*, *68*(2), 249–255. https://doi.org/10.1016/j.jfoodeng.2004.05.037

Liu, W., Zhang, M., Adhikari, B., & Chen, J. (2020). A novel strategy for improving drying efficiency and quality of cream mushroom soup based on microwave pre-gelatinization and infrared freeze-drying. *Innovative Food Science and Emerging Technologies*, *66*(September), 102516. https://doi.org/10.1016/j.ifset.2020.102516

Luo, N., & Shu, H. (2017). Analysis of Energy Saving during Food Freeze Drying. *Procedia Engineering*, *205*, 3763–3768. https://doi.org/10.1016/j.proeng.2017.10.330

Madrid, M., & Beaudry, R. (2020). Small fruits: Raspberries, blackberries, blueberries. In M. I. Gil & R. Beaudry (Eds.), *Controlled and Modified Atmospheres for Fresh and Fresh-Cut Produce* (Academic P, pp. 335–346). Elsevier. https://doi.org/10.1016/b978-0-12-804599-2.00020-x

Meulleneti, J. (1998). RELATIONSHIP BETWEEN SENSORY AND INSTRUMENTAL TEXTURE PROFILE ATTRIBUTES. *Journal of Sensory Studies*, *13*(1998), 77–93.

Mujumdar, A. S., Law, C. L., & Woo, M. W. (2015). Freeze Drying: Effects on Sensory and Nutritional Properties. In *Encyclopedia of Food and Health* (1st ed.). Elsevier Ltd. https://doi.org/10.1016/B978-0-12-384947-2.00327-5

Nooshkam, M., Varidi, M., & Bashash, M. (2019). The Maillard reaction products as food-born antioxidant and antibrowning agents in model and real food systems. *Food Chemistry*, *275*(September 2018), 644–660. https://doi.org/10.1016/j.foodchem.2018.09.083

Oliveira, N. L., Silva, S. H., Figueiredo, J. de A., Norcino, L. B., & Resende, J. V. de. (2021). Infrared-assisted freeze-drying (IRFD) of açai puree: Effects on the drying kinetics, microstructure and bioactive compounds. *Innovative Food Science and Emerging Technologies*, *74*(July), 10. https://doi.org/10.1016/j.ifset.2021.102843

Orrego, A. C. E. (2008). *Congelación y liofilización de alimentos* (UNIVERSIDAD NACIONAL DE COLOMBIA-GOBERNACIÓN DE CALDAS (ed.); 1st ed., Issue December). Artes Gráficas Tizan Ltda.

Pan, Z., & Atungulu, G. G. (2010). *Infrared Heating for food agricultural processing* (1st ed.). CRC Press.

Pawar, S. B., & Pratape, V. M. (2017). Fundamentals of Infrared Heating and Its Application in Drying of Food Materials: A Review. *Journal of Food Process Engineering*, *40*(1). https://doi.org/10.1111/jfpe.12308

Rastogi, N. K. (2021). Infrared Heating in Drying Operations. In *Innovative Food Processing Technologies: A Comprehensive Review* (pp. 1–21). Elsevier. https://doi.org/10.1016/b978-0-08-100596-5.22671-1

Ratti, C. (2013). Freeze drying for food powder production. In *Handbook of Food Powders: Processes and Properties* (1st ed., pp. 57–84). Woodhead Publishing Limited. https://doi.org/10.1533/9780857098672.1.57

Sakai, N., & Hanzawa, T. (1994). Applications and advances in far-infrared heating in Japan. *Trends in Food Science and Technology*, *5*(11), 357–362. https://doi.org/10.1016/0924-2244(94)90213-5

Salehi, F., & Kashaninejad, M. (2018). Modeling of moisture loss kinetics and color changes in the surface of lemon slice during the combined infrared-vacuum drying. *Information Processing in Agriculture*, *5*(4), 516–523. https://doi.org/10.1016/j.inpa.2018.05.006

Sandu, C. (1986). Infrared Radiative Drying in Food Engineering: A Process Analysis. *Biotechnology Progress*, *2*(3), 109–119. https://doi.org/10.1002/btpr.5420020305

Singh, V., Guizani, N., Al-Alawi, A., Claereboudt, M., & Rahman, M. S. (2013). Instrumental texture profile analysis (TPA) of date fruits as a function of its physico-chemical properties. *Industrial Crops and Products*, *50*, 866–873. https://doi.org/10.1016/j.indcrop.2013.08.039

Singleton, V. L., & Rossi, J. A. (1965). Colorimetry of Total Phenolics with Phosphomolybdic-Phosphotungstic Acid Reagents. *American Journal of Enology and Viticulture*, *16*(3), 144 LP – 158. http://www.ajevonline.org/content/16/3/144.abstract

Tonon, R. V., Brabet, C., & Hubinger, M. D. (2010). Anthocyanin stability and antioxidant activity of spray-dried açai (Euterpe oleracea Mart.) juice produced with different carrier agents. *Food Research International*, *43*(3), 907–914. https://doi.org/10.1016/j.foodres.2009.12.013

Waghmare, R. B., Perumal, A. B., Moses, J. A., & Anandharamakrishnan, C. (2021). Recent Developments in Freeze Drying of Foods. In *Innovative Food Processing Technologies* (Vol. 3, pp. 82–99). Elsevier. https://doi.org/10.1016/B978-0-12-815781-7.00017-2

Wang, H. C., Zhang, M., & Adhikari, B. (2015). Drying of shiitake mushroom by combining freeze-drying and mid-infrared radiation. *Food and Bioproducts Processing*, *94*(August), 507–517. https://doi.org/10.1016/j.fbp.2014.07.008

Wu, X., Zhang, M., & Bhandari, B. (2019). A novel infrared freeze drying (IRFD) technology to lower the energy consumption and keep the quality of Cordyceps militaris. *Innovative Food Science and Emerging Technologies*, *54*(December 2018), 34–42. https://doi.org/10.1016/j.ifset.2019.03.003

Wu, Y., Zhang, C., Huang, Z., Lyu, L., Li, J., Li, W., & Wu, W. (2021). The Color Difference

of Rubus Fruits is Closely Related to the Composition of Flavonoids including Anthocyanins. *LWT - Food Science and Technology*, 49. https://doi.org/10.1016/j.lwt.2021.111825

Yamashita, C., Chung, M. M. S., dos Santos, C., Mayer, C. R. M., Moraes, I. C. F., & Branco, I. G. (2017). Microencapsulation of an anthocyanin-rich blackberry (Rubus spp.) by-product extract by freeze-drying. *LWT - Food Science and Technology*, *84*, 256–262. https://doi.org/10.1016/j.lwt.2017.05.063

Zhang, Y., Zhu, G., Li, X., Zhao, Y., Lei, D., Ding, G., Ambrose, K., & Liu, Y. (2020). Combined medium- and short-wave infrared and hot air impingement drying of sponge gourd (Luffa cylindrical) slices. *Journal of Food Engineering*, *284*(17). https://doi.org/10.1016/j.jfoodeng.2020.110043